https://doi.org/10.5194/cp-2020-17
Preprint. Discussion started: 19 February 2020
© Author(s) 2020. CC BY 4.0 License.

Climate of the Past Discussions

PlioMIP2 simulations using the MIROC4m climate model

Wing-Le Chan[1], Ayako Abe-Ouchi[1,2]

[1]Atmosphere and Ocean Research Institute, The University of Tokyo, Kashiwa, 277-8564, Japan
[2]National Institute for Polar Research, Tachikawa, 190-8518, Japan

Correspondence to: Wing-Le Chan (wlchan@aori.u-tokyo.ac.jp)

Abstract. The second phase of the Pliocene Model Intercomparison Project (PlioMIP2) has attracted many climate modelling groups in its continuing efforts to better understand the climate of the mid-Piacenzian warm period (mPWP) when atmospheric CO_2 was last closest to present day levels. Like the first phase, PlioMIP1, it is an internationally coordinated initiative that allows for a systematic comparison of various models in a similar manner to PMIP. Model intercomparison and model-data comparison now focus specifically on the interglacial at marine isotope stage KM5c (3.205Ma) and experimental design is not only based on new boundary conditions but includes various sensitivity experiments. In this study, we present results from long-term model integrations using the MIROC4m atmosphere-ocean coupled general circulation model, developed at the institutes CCSR/NIES/FRCGC in Japan. The core experiment, with CO_2 levels set to 400ppm, shows a warming of 3.1°C compared to the Pre-Industrial, with two-thirds of the warming being contributed by the increase in CO_2. Although this level of warming is less than that in the equivalent PlioMIP1 experiment, there is a slightly better agreement with proxy sea surface temperature (SST) data at PRISM3 locations, especially in the northern North Atlantic where there were large model-data discrepancies in PlioMIP1. Similar changes in precipitation and sea ice are seen and the Arctic remains ice-free in the summer. However, unlike PlioMIP1, the Atlantic Meridional Overturning Circulation (AMOC) is now stronger than that of the Pre-Industrial, even though increasing CO_2 tends to weaken it. This stronger AMOC is a consequence of a closed Bering Strait in the PlioMIP2 paleogeography. Also, when present day boundary conditions are replaced by those of the Pliocene, the dependency of the AMOC strength on CO_2 is significantly weakened. Sensitivity tests show that lower values of CO_2 give a global SST which is overall more consistent with the PRISM3 SST field presented in PlioMIP1. Inclusion of dynamical vegetation and the effects of all realistic orbital configurations should be considered in future experiments using MIROC4m for the mPWP.

1 Introduction

The mid-Pliocene was the most recent period in the earth's history to have experienced sustained levels of atmospheric CO_2 similar to those of present day. Global temperatures are also estimated to have been 2-3°C higher than those of present day (Chandler et al., 2008). Various proxy evidence, including pollen assemblages (Brigham-Grette et al., 2013) and tetraether lipids (Crampton-Flood, 2017), have been used to reconstruct larger temperature changes at northern high latitudes. As a clear understanding of climate change in the near future becomes ever more important, scientists have also looked to warm climates

https://doi.org/10.5194/cp-2020-17
Preprint. Discussion started: 19 February 2020
© Author(s) 2020. CC BY 4.0 License.

Climate of the Past Discussions

of the past to validate model predictions and to quantify the forcings responsible for large climatic shifts. The mid-Pliocene has often been thought of as a good analogue for near-future climates, with formal assessments based on quantitative comparisons between past warm periods and Representative Concentration Pathway emission scenarios (Burke et al., 2018). The first studies of the mid-Pliocene using climate models were those of Chandler et al. (1994) whose results using the GISS AGCM showed a decrease in the equator-to-pole temperature gradient and of Sloan et al. (1996) who found a global surface temperature increase of 3.6°C with the NCAR GENESIS AGCM. These were eventually followed by studies using coupled atmosphere-ocean models, such as HadCM3 (Haywood and Valdes, 2004; Lunt et al., 2008) and NCAR CCMS3 (Jochum et al., 2009). Some of these studies investigated the specific effects of changing seaways and mountain uplifts which occurred during that time. Simultaneously, there have been on-going efforts with reconstructions of the mid-Pliocene climate using a multitude of marine and terrestrial proxy data. PRISM (Pliocene Research Interpretation and Synoptic Mapping) reconstructions of sea surface temperature (SST) and vegetation were first introduced in Dowsett et al. (1994).

The Pliocene Model Intercomparison Project (PlioMIP) was initiated at a time when climate models were increasingly used to simulate past climates to assess their performances by way of model intercomparison or model-data comparison (e.g. Braconnot et al., 2007). The first phase (Haywood et al., 2010, 2011), henceforth named PlioMIP1, focused on the mid-Piacenzian warm period (mPWP) within the mid-Pliocene, defined by PRISM as the interval between 3.264 and 3.025Ma. Adhering to the experimental designs specified in PlioMIP and using PRISM3D boundary conditions, models simulated an annual mean surface temperature increase of 1.8 to 3.6°C from Pre-Industrial values, in addition to the aforementioned decrease in the equator-to-pole temperature gradient Haywood et al. (2013). Despite this polar amplification, models were unable to replicate the scale of warming in the northern North Atlantic as suggested by PRISM3 proxy data (Dowsett et al., 2013). Subsequent model intercomparison studies yielded findings on the intensification of the East Asian monsoon during the mPWP (Zhang, R. et al., 2013), the different responses of the Atlantic Meridional Overturning Circulation (Zhang, Z. et al., 2013) and the importance of albedo feedbacks to high latitude warming (Hill et al., 2014), amongst other topics.

Lessons learnt and new insights gained from PlioMIP1 were applied to the second phase of the project, PlioMIP2 (Haywood et al., 2016), and an attempt was made to address shortcomings from the design in the first phase, namely, uncertainties in the boundary conditions, data and model physics, which could contribute to model-data discord. New reconstructions for paleogeography, land surface elevation and ice sheet distribution as part of PRISM4 were used as boundary conditions for PlioMIP2 experiments (Dowsett et al., 2016), including closure of the Bering Strait and a smaller Greenland ice sheet restricted to the eastern part of the island. As opposed to a time slab or interval, the reconstructions now focus on a particular time slice, the interglacial peak MIS KM5c (3.205Ma), which has an orbital forcing close to that of present day. Additionally, PlioMIP2 forms part of the fourth phase of the Paleoclimate Modelling Intercomparison Project (PMIP4) and the sixth phase of the Coupled Model Intercomparison Project (CMIP6) (Kageyama et al, 2018).

PlioMIP2 also laid out plans for non-core sensitivity experiments to investigate the effects of individual boundary conditions and to account for the uncertainty in greenhouse gas levels. Estimates of CO_2 for this period from different marine proxy records vary widely, from 250 to 450ppm (Fedorov et, 2013), including uncertainties in individual sources. Values in

https://doi.org/10.5194/cp-2020-17
Preprint. Discussion started: 19 February 2020
© Author(s) 2020. CC BY 4.0 License.

Climate of the Past Discussions

the upper half of that range are inferred from alkenone-derived $\delta^{13}C$ and foraminiferal $\delta^{11}B$ (Seki et al., 2010), stomatal properties of leaves (Kürschner et al., 1996) and marine plankton $\delta^{13}C$ (Raymo et al., 1996). Estimates from the lower half are derived from B/Ca ratios in foraminifera (Tripati et al., 2009) and other foraminiferal $\delta^{11}B$ (Bartoli et al., 2011). The core experiment in PlioMIP2 has a setting of 400ppm for CO_2, which accounts for greenhouse gas forcing from all sources, and is close to the PlioMIP1 value.

The main aim of this study is to present results of both core and some non-core PlioMIP2 experiments using MIROC4m. With these results, we investigate the differences in the climate state when switching from PlioMIP1 boundary conditions to PlioMIP2. Using results from non-core experiments, we examine the individual effects of increasing CO_2 and of introducing PlioMIP2 boundary conditions. We also compare proxy data with our model results, including those from sensitivity experiments using a range of CO_2 levels.

2 Model description

In the present study, the experiments have been carried out with the coupled atmosphere-ocean general circulation model, MIROC4m (The Model for Interdisciplinary Research on Climate), a mid-resolution model developed jointly by the institutes CCSR, FRCGC and NIES in Japan (K-1 model developers, 2004). This model has previously been used to study a variety of climate states, for example, future RCP4.5 and RCP8.5 scenarios (Bakker et al., 2016), the mid-Holocene (Ohgaito et al, 2013), the Last Glacial Maximum (Yanase and Abe-Ouchi, 2007) and the mPWP (Chan et al., 2011). A higher resolution of the same model was included in the Fifth Assessment Report of the Intergovernmental Panel on Climate Change (IPCC, 2013). Note that this model is not a contributing member to PMIP4/CMIP6, and so results in this study are confined to PlioMIP2.

The model consists of an atmosphere-land-river component and a sea ice-ocean component, with the air-sea exchange of momentum, heat and water occurring at the air-sea ice interface. At ice-free grid cells, exchange still occurs via the sea ice subcomponent but the flux to the ocean remains unchanged. Below is a brief description and readers should refer to K-1 model developers (2004) and the references contained within for further details.

The atmospheric component is identical to the AGCM described in Numaguti et al. (1997), namely, CCSR/NIES/FRCGC AGCM5.7b. The horizontal resolution is set to T42, which corresponds to a grid size of approximately 2.8° longitude and latitude and the vertical set to 20 σ levels. USGS GTOPO30 is used to generate the surface elevation. The level 2 scheme of the turbulence closure model by Mellor and Yamada (1982) is used for sub-grid vertical fluxes of prognostic variables. A radiative transfer scheme (Nakajima et al., 2000) based on the two-stream discrete ordinate and k-distribution methods is employed. Optical parameters for water cloud, ice cloud, soil dust, black carbon, organic carbon, sulfate and sea salt are also included. Classification of aerosols is based on Spectral Radiation-Transport Model for Aerosol Species (SPRINTARS) (Takemura et al., 2000).

https://doi.org/10.5194/cp-2020-17
Preprint. Discussion started: 19 February 2020
© Author(s) 2020. CC BY 4.0 License.

Climate of the Past Discussions

The land-surface model used is Minimal Advanced Treatments of Surface Interaction and Runoff (MATSIRO) (Takata et al, 2003), whose horizontal resolution is the same as that of the atmospheric component. Water and heat exchange between the land surface and atmosphere, and runoff flux to a river routing model are represented. Prognostic variables include canopy water content, canopy temperature and soil moisture. Land-cover classification is derived from USGS GLCC (Global Land Cover Characterization). See Chan et al. (2011) for the present-day vegetation distribution.

The ocean component is basically version 3.4 of the CCSR Ocean Component Model (COCO) (Hasumi, 2000). The horizontal grid has 256x192 points so that each grid point is spaced equally at 1.40625° in the longitudinal direction. In the latitudinal direction, resolution is highest in the tropics (0.56°) and lowest at the polar regions (1.4°). The are 43 vertical levels, including 8 σ levels near the sea surface. The Bering Strait throughflow is fully represented but the Hudson Bay and the Mediterranean Sea are treated as isolated lakes with heat and salinity exchanged with the open seas by a 2-way linear damping. A simple, vertical adjustment is applied, whereby unstable water columns are homogenised instantaneously. Vertical mixing of sea tracers and momentum use viscosity and diffusion coefficients calculated by Noh and Kim (1999). While there are no changes to the model as used in PlioMIP1, it should be noted that a larger Gent-McWilliams coefficient has been used in other more recent published work using MIROC4m (Obase and Abe-Ouchi, 2019, Sherriff-Tadano and Abe-Ouchi, 2020). This coefficient which refers to the horizontal diffusion of the isopycnal layer thickness is set to $300 m^2/s$ in the present study.

Sea ice concentration, thickness and horizontal velocities are calculated in the sea ice model. The equation of momentum includes an advection term, a Coriolis term, an acceleration term due to the slope of the sea surface, an internal stress term and an external forcing term derived from wind stress and ice-ocean drag.

3 Experimental design

The nomenclature used for the experiments follows that specified for PlioMIP2 (Haywood et al, 2016), that is, it takes the form Ex^c, where c is the concentration of CO_2 in ppm, and x can be any combination of the Pliocene boundary conditions. With present day boundary conditions only, x is null, otherwise it can be o (Pliocene orography, bathymetry, land-sea mask, lakes and soils combined) and/or i (Pliocene ice sheets).

Altogether, results from 8 experiments are included in this study. Firstly, there are the two core experiments, the Pre-Industrial (E^{280}) and a Pliocene time slice (Eoi^{400}), which all modelling groups participating in PlioMIP2 are expected to run. Secondly, with the Pre-Industrial set-up, atmospheric CO_2 levels are increased to 400ppm and double that of the Pre-Industrial (E^{400} and E^{560}). Thirdly, at the Pliocene time slice, atmospheric CO_2 levels are changed to 280ppm, 350ppm and 450ppm (Eoi^{280}, Eoi^{350} and Eoi^{450}). These two groups form part of the Tier 1 and 2 experiments. Fourthly, we include an experiment with all boundary conditions set to those of the mPWP in PlioMIP1 and name this Eplio1 as it is not formally part of PlioMIP2. In the core, Pre-Industrial experiment, atmospheric CO_2, CH_4 and N_2O levels were initially set to those used for the MIROC4m experiments in PlioMIP1 (see Chan et al., 2011), and these levels differed slightly to the specifications set in PlioMIP2. All the other experiments in this study subsequently followed the Pre-Industrial, including the double CO_2 experiment in which

https://doi.org/10.5194/cp-2020-17
Preprint. Discussion started: 19 February 2020
© Author(s) 2020. CC BY 4.0 License.

Climate of the Past Discussions

CO_2 is set to 571ppm. In order that MIROC4m results may be compared systematically with data from other modelling groups in future studies, the 8 experiments are continued for a further 1,000 model years with the three greenhouse gas levels set to those specified in Haywood et al. (2016). Final CO_2 levels and boundary conditions for each experiment are listed in Table 1. Common to all experiments are the other greenhouse gases, astronomical parameters and the solar constant which are listed in Table 2.

3.1 Pre-Industrial (E^{280}) and increased CO_2 experiments (E^{400} and E^{560})

These 3 experiments with present day land topography were run previous to this study. The CO_2 level for the Pre-Industrial (E^{280}) is initially set to approximately 285ppm, in accordance to previous MIROC4m experiments, and thus double the Pre-Industrial level is set to 571ppm. The model was integrated for 1220, 2000 and 2920 years for E^{280}, E^{400} and E^{560}, respectively, using these old greenhouse gas levels. The time series of the AMOC and global temperatures for the last 1000 years are shown on the extreme left in Figure 2. For this study, these experiments are continued for another 1000 model years with the greenhouse gases changed to levels specified in PlioMIP2; the time series for these 1000 years are plotted on the right-hand side of Figure 2.

3.2 Core Pliocene (Eoi^{400}) and related experiments with different CO_2 levels (Eoi^{280}, Eoi^{350} and Eoi^{450})

With greenhouse gas levels initially set to their previous values, the core experiment, Eoi^{400}, and the same experiment with Pre-Industrial CO_2 levels, Eoi^{280}, start from E^{280} and the model is integrated for 3000 and 1500 years, respectively. At the end of 3000 years, Eoi^{350} and Eoi^{450} branch off Eoi^{400}; the model for these two branches is integrated for 2000 years. Then as before, with greenhouse gas levels modified to PlioMIP2 values for these 4 experiments, the model is integrated for a further 1000 years. The full, enhanced boundary conditions from Haywood et al. (2016) are employed, in particular, the Pliocene minus Modern topography anomaly, as shown in Figure 1, is applied to the existing MIROC4m land elevation. For consistency we apply the same vegetation distribution as that in the PlioMIP1 study by Chan et al. (2011), derived from Salzmann et al. (2008). The vegetation is extended in several regions where the land mask differs from that of PlioMIP1, for example, over an expanded Indonesia, over Beringia, resulting from a closed Bering Strait, and across parts of Greenland where the ice sheets are now specified to be smaller than that of PlioMIP1. In addition, several lakes have now been included on the African continent. The bathymetry is modified by the usual anomaly method, although a separate experiment was carried out without such modifications, resulting in no noticeable differences in the climate. Soil types are changed according to their texture.

3.3 Pliocene with PlioMIP1 boundary conditions (Eplio1)

For the lone experiment with PlioMIP1 boundary conditions and CO_2 level set to 405ppm, the model is initialised with Pre-Industrial conditions and integrated for 3000 years before the other greenhouse gas levels are changed to PlioMIP2 values for a further 1000 years. As in our original PlioMIP1 experiment (Chan et al., 2011), there are no modifications made to the bathymetry, soil types or lakes.

https://doi.org/10.5194/cp-2020-17
Preprint. Discussion started: 19 February 2020
© Author(s) 2020. CC BY 4.0 License.

Climate of the Past Discussions

4 Results and discussion

Henceforth, we call all experiments with PlioMIP1 or PlioMIP2 boundary conditions as simply "Pliocene experiments", irrespective of CO_2 level. Analyses are mostly based on the last 100 years of the model integration for each experiment and focus on the differences between the Pliocene experiments, especially the core, default Eoi^{400} experiment, and the Pre-Industrial E^{280} experiment. We also examine the Pliocene climate for a range of CO_2 levels and determine how the Pliocene experiments, in particular the core experiment, compares with proxy data for surface air and sea surface temperatures.

4.1 Surface air temperature

The changes in the annual mean surface air temperature (SAT) from Pre-Industrial values are shown in Figure 3. When only the CO_2 level is increased (Figure 3a), temperatures increase fairly uniformly, in comparison to the other experiments. E^{560}-E^{280} is not shown in this figure, but spatially, it resembles E^{400}-E^{280}. Temperature increases are slightly higher over land, with the smallest increases over central Africa and south-east Asia. Over the oceans, there are small regions, mainly over the Greenland Sea, where temperature changes are small, or even negative, and this is also noticeable to some extent in the other experiments. The largest temperature increases occur around the edge of Antarctica and across the Barents Sea. When only Pliocene vegetation, ice sheets, land configuration and elevation are introduced, and the CO_2 level is left unchanged, as in Eoi^{280}-E^{280} (Figure 3c), the largest temperature increases can be found in the exact regions where ice sheets have been removed and land elevation is consequently lowered, that is, West Antarctica, the coastal regions of East Antarctica just to the south of Australia, and Greenland. Conversely, over the interior of the Antarctic continent, there are also locations where the temperature has decreased because the land elevation has increased while ice sheet is still present. Combining all Pliocene boundary conditions with increased CO_2, the spatial distribution resembles that of Eoi^{280}-E^{280}, with CO_2 providing an even increase in temperature everywhere. This near-linearity of the combined effects of CO_2 and Pliocene land conditions is also reflected in the globally averaged temperature increase shown in Table 3. This increase, the global SAT anomaly, for E^{400} and Eoi^{280} is 2.0°C and 1.1°C, respectively, and that for Eoi^{400} is 3.1°C, which corresponds to a near-zero residual from non-linear effects, similar to the findings of Kamae et al. (2016) who further decomposed the Pliocene land conditions into ice sheets and all other effects. Others find that the combined effects are less than the sum of the individual effects (Hunter et al., 2019; Chandan and Peltier, 2018). The temperature increase in Eoi400 is not as large as that in the PlioMIP1 experiment. PlioMIP2 temperature increases in both the northern high latitudes and the tropics are smaller and this may be at least partly a result of the increased elevation across most of the northern hemisphere, especially over North America. On the other hand, PlioMIP1 temperature increase is smaller over the southern high latitudes. Overall, the PlioMIP1 temperatures lie in between those of PlioMIP2 with CO_2 set to 400 and 450ppm.

The globally averaged SAT from PlioMIP has been used to estimate the Earth system sensitivity (ESS), which, unlike the climate sensitivity (CS), takes into account feedbacks operating over longer timescales (Lunt et al., 2009). From E^{280} and E^{560}, CS is estimated to be 3.9, and using Eplio1 and Eoi^{400}, ESS is estimated to be 6.6 and 6.0, respectively, and the ESS/CS

https://doi.org/10.5194/cp-2020-17
Preprint. Discussion started: 19 February 2020
© Author(s) 2020. CC BY 4.0 License.

Climate of the Past Discussions

ratio 1.7 and 1.5, respectively. All these values compare quite well with the PlioMIP2 multi-model mean values (Haywood et al., 2020).

Figure 4 shows the zonal mean surface air temperature increase from E^{280}. The near-uniform increase outside the polar regions when only CO_2 is changed is evident (see the red and purple lines). For all other experiments, there is a bias in the northern hemisphere because of the larger continents. In the northern polar region, peak temperature increase is seen at 75°N. However, in the southern polar region, peak temperature increase shifts from 65°S to 75°S with the inclusion of Pliocene land elevation and reduced ice sheets. For the Pliocene experiments, Eoi^{350}, Eoi^{400} and Eoi^{450}, the increase in zonal temperature with an increase of 50ppm in CO_2 is limited to less than 1°C at low and mid-latitudes, and at most 1.5°C at the polar regions. This is relatively uniform in comparison to results from models like IPSL-CM5A2 which shows a fairly small uniform change from Eoi350 to Eoi400, except at the northern high latitudes where there is a sharp change of up to 2.5°C (Figure 11c of Tan et al., 2020).

The seasonal surface air temperature anomalies for Eoi^{400} are shown in Figure 5. There is little seasonal change over north Africa and much of the oceans. Throughout the year, temperature increases over Greenland remain large. However, there are distinct seasonal changes at high latitudes elsewhere, for example, the small temperature increase in the Arctic region during the summer, followed immediately by the extremely large temperature increase during the autumn. The Hudson Bay shows a large temperature reduction during winter because it has been replaced by land which cannot stabilise the surface air temperature as much as water can (Hunter et al., 2019). Conversely, by the same reasoning, a large temperature increase is seen over the Hudson Bay during the summer. Another region where the temperature reduces is the zonal strip in Africa at latitude 15°N during the summer. This is similar to what was seen in the early work of Chandler et al. (1996) who attributed this feature to a weakening of the Hadley circulation. Both the summer cooling over this part of Africa and the Indian subcontinent are also clearly seen in Hunter et al. (2019).

4.2 Sea surface temperature

Annual mean sea surface temperature (SST) anomalies, shown in Figure 6, are similar to SAT anomalies. With only an increase in CO_2 (Figure 6a), there is a uniform increase in SST, except in the eastern Pacific and Indian Ocean sectors of the Southern Ocean, in the north-west Pacific Ocean and in the Greenland Sea. The inclusion of all other Pliocene boundary conditions leads to more extreme SST increases over the northern mid to high latitudes, as well as the western half of the Indian Ocean. The Greenland Sea is the only region where SST decreases whether by increasing CO_2 to 400ppm (Figure 6a) or by introducing Pliocene boundary conditions (Figure 6c) and this cooling persists in all the Pliocene experiments. The global SST for Eoi^{400} is 19.0°C (Table 3), slightly lower than that for the PlioMIP1 experiment (19.2°C). It is later shown in Figure 15(b) that SST is much lower in Eoi^{400} than in Eplio1 in the Barents Sea, along the north-west Pacific coastal regions, but much higher in the Labrador Sea, the eastern North Atlantic Ocean and parts of the Southern Ocean. The difference in the Barents Sea SST of the two experiments could be explained by the higher land elevation over northern Europe in PlioMIP2

https://doi.org/10.5194/cp-2020-17
Preprint. Discussion started: 19 February 2020
© Author(s) 2020. CC BY 4.0 License.

Climate of the Past Discussions

which would lead to SAT lower than those in Eplio1 in the same way higher land elevation over North America leads to SAT there being lower in Eoi^{400} than in Eplio1.

4.3 Precipitation

For the Pliocene experiments, the fractional increase in the annual mean precipitation (Figure 7) is greatest over most of Antarctica, northern Africa, the Indian Ocean, central Asia and at the northern high latitudes, in particular, across Greenland and northern Canada. Consequently, the sea surface salinity (not shown) in the Indian Ocean reduces by a large amount. Conversely, the precipitation decreases most noticeably over the oceans elsewhere, at the tropics and subtropics, in addition to the Greenland Sea where SAT decreases. Over land, the precipitation decreases across south-east North America and southern Africa. As the CO_2 level is increased, these changes are accentuated and the globally averaged precipitation increases (column 8, Table 3). The opposing changes across northern Africa and the northern South Atlantic Ocean is indicative of a northward shift of the Intertropical Convergence Zone. It can be seen from a comparison of E^{400}-E^{280} (Figure 7a) and Eoi^{280}-E^{280} (Figure 7c) that most of these changes in precipitation occur as a result of the Pliocene boundary conditions, rather than the change in CO_2. The increase in CO_2 is responsible for a moderate increase in precipitation over the whole of Antarctica and for a small decrease over northern Africa, opposite to the effect of the Pliocene boundary conditions. The spatial changes in the PlioMIP1 experiment are similar to those in Eoi^{400}, with the global changes in precipitation also being similar (Table 3). As with SAT, the globally averaged precipitation in Eoi^{400} is larger than that in E^{280}, with CO_2 contributing about two-thirds of the total increase.

4.4 Sea ice and ocean mixed layer depth

The total sea ice area in the polar regions is depicted in Figure 8. In the Arctic, during March when the sea ice area is at its greatest, there is a gradual decrease in area as CO_2 is increased, whether Pre-Industrial or Pliocene boundary conditions are used. The sea ice area in Eplio1 is actually larger than any of the other Pliocene experiments because the land area around the Arctic is smaller in Eplio1, as can be seen later in Figure 9 – the Bering Strait is open, the Hudson Bay is still set as open water and the Labrador Sea is larger and connected to the Arctic Ocean. During September, when the sea ice area is at its smallest, a similar trend is observed. The Arctic Ocean is ice-free in Eplio1, Eoi^{400} and Eoi^{450}. In the Antarctic, during September, the decrease in sea ice area as CO_2 increases is much more drastic. The Antarctic sea ice area when the CO_2 level is doubled is also much lower than that of any of the Pliocene experiments. Unlike the Arctic, the sea ice area in Eplio1 and Eoi^{400} are similar as the Antarctic coastlines in the two cases do not differ by much. The same behaviour is observed in March, although unlike in the Arctic, the Antarctic is never ice-free.

The sea ice extent in the Arctic and the mixed layer depth (MLD) in the surrounding regions during March are shown in Figure 9. The definition of the MLD follows that of Oka et al. (2006), i.e. the depth at which σ_θ, the potential density anomaly, differs from the surface value by 0.1. The sea ice extent here is largely unaffected by the Pliocene boundary conditions alone and only recedes near the north-west Pacific coastline and in the Barents Sea as CO_2 is increased. The MLD,

https://doi.org/10.5194/cp-2020-17
Preprint. Discussion started: 19 February 2020
© Author(s) 2020. CC BY 4.0 License.

Climate of the Past Discussions

on the other hand, also responds to changes in CO_2 alone. In E^{280}, the MLD is large west of the British Isles and everywhere south of the sea ice in the Atlantic. As CO_2 is increased (E^{400} and E^{560}), the MLD decreases in the former but increases over a larger area south of Greenland. With Pliocene boundary conditions, a large MLD is also exhibited in the same area south of Greenland, even in Eoi^{280}. However, the MLD west of the British Isles remains large while a large MLD is now seen south of Alaska. These results suggest an increase in downwelling south of Greenland. The sea ice extent and MLD in the Antarctic during September are shown in Figure 10. With present day boundary conditions (E^{280}, E^{400} and E^{560}), the MLD is extremely large in the Atlantic sector of the Southern Ocean, even below parts of the sea ice in E^{280}, suggesting the formation of dense water due to brine rejection. In the Pliocene experiments, this large MLD is absent, while in the other region where the MLD is large with present day boundary conditions, i.e. the eastern South Pacific, it is reduced.

4.5 Atlantic meridional overturning circulation

The Atlantic meridional overturning circulation (AMOC) is shown in Figure 11 and the AMOC index, defined as the maximum streamfunction value, in the last column of Table 3. Increasing the CO_2 level alone has a tendency to weaken the AMOC. As the overturning cell becomes shallower, the underlying Antarctic Bottom Water extends further northward. In addition, the anti-clockwise overturning cell north of 65°N strengthens, contributing to increased convection and deepwater formation in the Labrador Sea, as indicated by the MLD in Figure 9. A comparison of Eoi^{280} with E^{280} shows that similar changes occur when only the Pliocene boundary conditions are applied, except that the AMOC index increases by nearly 0.7Sv, despite shoaling of the AMOC. Thus, increasing CO_2 and applying Pliocene boundary conditions have an opposite effect on the AMOC index, but up to 450ppm CO_2, the indices for all the Pliocene experiments are still greater than that for E^{280}. Note that the degree of weakening in the AMOC as CO_2 increases seem to be highly dependent on the boundary conditions. With present day boundary conditions, from E^{280} to E^{400}, the AMOC index decreases by 0.8Sv, whereas in the corresponding Pliocene experiments, Eoi^{280} and Eoi^{400}, there is only a decrease of approximately 0.2Sv (Table 3).

A comparison of Eoi^{400} and Eplio1 shows that while the AMOC cell extends to similar depths and the circulation in the other two cells change little, the AMOC index with PlioMIP2 boundary conditions is larger than that with PlioMIP1, 20.0Sv versus 17.8Sv. While we have not performed specific sensitivity experiments to see what difference between the PlioMIP1 and PlioMIP2 boundary conditions is exactly responsible for this difference in the AMOC index, we did perform some (not shown) with a Pre-Industrial background climate and looked at the effects of closing the Bering Strait and the Canadian Arctic Archipelago Straits (CAAS) closed. We find that, as in Pliocene studies by Otto-Bliesner et al. (2017), closure of the Bering Strait, irrespective of the state of the CAAS, leads to a stronger AMOC. Closing the Bering Strait inhibits the transport of freshwater from the North Pacific Ocean via the Arctic Ocean and increases the AMOC index by 1-2Sv in the MIROC4m experiments, and so it likely explains the difference between Eoi^{400} and Eplio1. This increase is sufficient to give a stronger Pliocene AMOC when compared to the Pre-Industrial, a result which is opposite to when using PlioMIP1 boundary conditions and which is consistent with recent PlioMIP2 simulations with other models (e.g. Chandan and Peltier, 2017; Tan et al., 2019; Hunter et al., 2019; Li et al., 2020).

https://doi.org/10.5194/cp-2020-17
Preprint. Discussion started: 19 February 2020
© Author(s) 2020. CC BY 4.0 License.

Climate of the Past Discussions

4.6 Meridional heat transport

Figure 12(a) shows the meridional ocean heat transport in the Atlantic Ocean for E^{280}. The transport peaks at around 0.7PW, near latitude 15°N. Figure 12(b) shows the difference between the same heat transport in the Pliocene experiments and E^{280}. In all the Pliocene experiments, there is a reduction in the heat transport at all latitudes, with the greatest reduction at the equator for experiments using PlioMIP2 boundary conditions. For these four PlioMIP2 Pliocene experiments, there does not appear to be any general trend as the CO_2 level is increased. For example, Eoi^{450} has a significantly lower heat transport compared to the others south of the equator, whereas at the northern low to mid-latitudes, Eoi^{450} values are rather close to those of Eoi^{400} and it is the Eoi^{280} values that stray from the rest. It can also be seen that there is a marked difference between the heat transport in Eplio1 and those using PlioMIP2 boundary conditions. At all latitudes south of 30°N, heat transport in Eplio1 is about 0.1PW lower than that of E^{280}. Irrespective of CO_2 levels, this larger difference can mostly be attributed to the differences between the PlioMIP1 and PlioMIP2 boundary conditions, as can the difference between the AMOC index of Eplio1 and those of the PlioMIP2 Pliocene experiments. However, as noted in the latter experiments, the northward heat transport decreases even though the AMOC index increases, albeit to a relatively small degree. While these two properties are commonly thought of as being positively correlated to each other, Sévellec and Fedorov (2016) show that this is not always the case.

Figure 13 shows the total meridional heat transport in a similar way, but for the whole climate system, combining atmosphere and ocean. For all Pliocene experiments, northward heat transport is reduced in the northern hemisphere, while southward heat transport is increased in the southern hemisphere. How these individual experiments differ from one another depends on the hemisphere. Firstly, with PlioMIP2 boundary conditions, as the CO_2 level is increased, there is a clear, monotonous trend with the magnitude of the northward heat transport anomaly reducing in the northern hemisphere. The opposite trend is seen in the southern hemisphere as southward heat transport increases with CO_2. Eoi^{400} represents a half-way mark whereby the bold green line in Figure 13(b) is roughly symmetric across the equator. Secondly, Eplio1 aligns very closely with Eoi^{400} in the southern hemisphere, whereas in the northern hemisphere, Eplio1 sets itself apart from the other Pliocene experiments and its heat transport reduces much less.

4.7 Comparison with surface air temperature proxy data

In Figure 14, the annual mean SAT from the Pliocene experiments and E^{280} are compared with proxy data at certain locations, as compiled by Salzmann et al. (2013). The red symbols refer to the PlioMIP2 Pliocene experiments, with the lower and higher horizontal red lines referring to 350ppm and 450ppm CO_2, respectively. For most locations, SAT from these experiments show the correct tendency and agree better with the proxy data than E^{280}. Locations where the Pliocene values do not match proxy data as well as E^{280} values include Rio Maior, Yorktown and Pinecrest, where the Pliocene values are too high and proxy data values are very close to E^{280} values. However, the biggest discrepancies are seen in the Charan Basin and Lake Baikal, but even here, the Pliocene values match proxy data better than E^{280} values. Moreover, the Pliocene model values

https://doi.org/10.5194/cp-2020-17
Preprint. Discussion started: 19 February 2020
© Author(s) 2020. CC BY 4.0 License.

Climate of the Past Discussions

at these two locations are very close to the CCSM4 model results in Table 4 of Chandan and Peltier (2017). There are many locations where the Pliocene SAT, in particular that of Eoi^{400}, fall within the proxy data uncertainty range, which, in turn, is significantly higher than the E^{280} values, eg Andalucia G1, Habibas and Nador. Eplio1 values, for the most part, are similar to Eoi^{400} or Eoi^{450} values. Thus, in general, the Pliocene experiments show good agreement with the proxy data, but there does not appear to be any particular value of CO_2 which gives the best fit.

4.8 Comparison with sea surface temperature proxy data

PRISM SST proxy data from a variety of marine sources have formed an integral part of PlioMIP, as boundary conditions for AGCM experiments in the first phase and, more importantly, as part of data-model comparison. Figure 15(a) compares the annual mean Eoi^{450}-E^{280} SST anomalies with the corresponding anomalies from PRISM3 sites where the colour refers to the difference between these two anomalies, with yellow, orange and red meaning model SST anomalies are greater. The symbols show whether the proxy anomalies suggest a warmer Pliocene (triangles) or a cooler Pliocene (circles). Only a few PRISM3 sites show a cooler Pliocene, at low latitudes, and Eoi^{400} does not replicate this cooling, especially in the Indian Ocean. In general, there is good agreement in the Southern Ocean where proxy data suggest a warmer Pliocene. In the northern hemisphere, where PRISM3 sites also suggest a warmer Pliocene, Eoi^{400} overestimates the SST increase by up to 3°C in parts of the southern North Atlantic. As with model results from PlioMIP1, the large degree of warming in the northern North Atlantic and Greenland Sea is not replicated (blue triangles). A comparison of Eoi^{400} and Eplio1 SST anomalies is shown by the colours in Figure 15(b). SST anomalies in Eoi^{400} are larger mainly in the Indian and Pacific sectors of the Southern Ocean, the eastern Atlantic Ocean and the Labrador Sea. While the SST anomalies in much of the northern North Atlantic and the Barents Sea are lower in Eoi400 compared to Eplio1, the Eoi^{400} values at the PRISM3 sites are actually higher, and thus agree better with the proxy data, as shown by the yellow triangles.

For a more global sense of how the various Pliocene experiments compare with the proxy data, we refer back to the global PRISM3 SST field which was used as boundary conditions for AGCM experiments in PlioMIP1 and list the spatially and annually averaged model-data difference in Table 4. The caveat here is that this global SST field is reconstructed from data at a finite number of sites for February and August using interpolation and extrapolation, and that there are regions where data are sparse (Dowsett et al., 1999). Comparing Eplio1 and Eoi^{400}, we see that the former matches the proxy data better at northern high latitudes, and even better at southern high latitudes (a difference of only 0.04°C). On the other hand, the latter shows a smaller discrepancy at the tropics and low latitudes (30°S-30°N) where the larger surface area means that, globally speaking, Eoi^{400} gives a better fit (a difference of 0.76°C). Next, a comparison of Eoi^{350}, Eoi^{400} and Eoi^{450} shows that, while there is a trend in the model-data difference as CO_2 is reduced, there is no particular level at which the difference is small at the three latitudinal ranges in Table 4. Since the global difference is determined more by the low latitudes, Eoi^{350} gives the best global fit (a difference of 0.14°C). It is worth noting that not only does Eoi^{280} give the best fit at low latitudes, but bucks the trend at the northern high latitudes where the discrepancy is smaller than that for Eoi^{350}. For reference, the discrepancies

https://doi.org/10.5194/cp-2020-17
Preprint. Discussion started: 19 February 2020
© Author(s) 2020. CC BY 4.0 License.

Climate of the Past Discussions

between the model and proxy SST anomalies at the PRISM3 sites for different CO_2 levels are shown in Supplementary Figure 1.

We also include a similar comparison between model results and the newer PRISM4 proxy SST data sets (Foley and Dowsett, 2019) in Supplementary Figure 2. The degree of warming in Eoi^{400} is much less than that suggested by PRISM4 proxy data in the Atlantic sites, especially at northern high latitudes again, and also near southern Africa. Slightly higher warming in Eoi^{400} is generally seen in the other sites, mostly located at low latitudes. The PRISM4 data used here refer to the broader 30ka interval, but alternative data for a 10ka interval give the same conclusions. Qualitatively speaking, at least, these results are similar to those obtained from the multi-model mean in Figure 8(c) of Haywood et al (2020).

5 Summary and conclusions

In the present study, we have shown some basic results from the core PlioMIP2 experiment using the MIROC4m AOGCM, compared them to results from both the PlioMIP1 experiment and some other Tier 1 and Tier 2 PlioMIP2 sensitivity experiments. Additionally, we have evaluated the consistency between these experimental results and some temperature proxy data from marine and terrestrial sources.

For the core experiment, PlioMIP2 boundary conditions produce a global temperature increase smaller than that with PlioMIP1 and it can be assumed that the CO_2 level has little effect as it differs only slightly in the two phases of PlioMIP. The difference in the results from these two experiments is not uniform as greater warming is seen in PlioMIP2 in parts of the northern high latitudes and of the Southern Ocean. Moreover, PlioMIP2 SSTs actually reconcile better with proxy-derived values at PRISM3 sites in the northern North Atlantic and Greenland Sea, albeit to a very small degree, although the large discord in the northern North Atlantic Ocean SSTs still remains. For SAT, both PlioMIP1 and PlioMIP2 values show fairly good agreement with terrestrial proxy data. Northern polar amplification is slightly less in PlioMIP2, but still, zonal SAT increases are more than double that of the low latitudes. Our sensitivity experiments have only distinguished between the two forcings from CO_2 and Pliocene boundary conditions and we have not considered the effects from the ice sheets, orography and vegetation separately. CO_2 accounts for two-thirds of the total surface air temperature and precipitation increase. Unlike PlioMIP1, the AMOC in PlioMIP2 is stronger compared to the Pre-Industrial for MIROC4m, which is in line with other model results published so far in PlioMIP2. The strengthening of the AMOC from PlioMIP1 to PlioMIP2 is tied to the closure of the Bering Strait.

We have also looked at the mid-Pliocene climate within a range of CO_2 values. While the expected trends are seen, such as the increase in global temperature and precipitation with CO_2, of much importance is the comparison with proxy-derived data. Mismatches between Eoi^{400} and proxy-derived SSTs at low and high latitudes are of the opposite sign, and data in both regions cannot be simultaneously reconciled simply by changing the CO_2 value. However, from a global perspective, a value below 400ppm leads to a better overall fit. From these CO_2 sensitivity experiments, we also find that, not only does

https://doi.org/10.5194/cp-2020-17
Preprint. Discussion started: 19 February 2020
© Author(s) 2020. CC BY 4.0 License.

Climate of the Past Discussions

the AMOC strength decrease with increasing CO_2, but that this dependency on CO_2 is weaker when Pliocene boundary conditions are used.

Our experiments have not included dynamical vegetation but previous research employing the same model coupled to a dynamic global vegetation model have shown that such vegetation feedback can amplify both warming in the mid-Holocene (O'ishi and Abe-Ouchi, 2011) and cooling in the cold climate of the LGM (O'ishi and Abe-Ouchi, 2013), especially at northern high latitudes. Subsequent Pliocene-related MIROC4m climate simulations will include a configuration with dynamical vegetation. Other recent studies have incorporated the effects of orbital forcing in simulations of the mPWP, with modelled climate, ice sheets and vegetation exhibiting strong regional variations associated with orbital parameters, whether as time-dependent forcing in transient simulations (Willeit et al., 2013) or fixed to minimum or maximum forcings (Dolan et al., 2011). While using present-day orbital parameters for the KM5c interglacial peak appears valid, at least with fixed vegetation (Hunter et al., 2019), an investigation of the mPWP as a whole necessitates more realistic orbital parameters, even when restricted to interglacial peaks (Prescott et al., 2018). This should be borne in mind when considering paleoclimate modelling experiments such as those for the mPWP.

Data availability

Data files containing the PlioMIP2 boundary conditions are directly accessible from the USGS PlioMIP2 website, https://geology.er.usgs.gov/egpsc/prism/7_pliomip2.html. Data for most experiments in this study are available on the PlioMIP2 data repository at the University of Leeds, sftp://see-gw-01.leeds.ac.uk. Request for access should be directed to A.M. Haywood. For all other data, readers are asked to contact the lead author, W.-L. Chan (wlchan@aori.u-tokyo.ac.jp).

Author contributions

Both authors contributed to the writing of the paper and discussions. WLC set up and carried out the experiments, wrote the first draft of the manuscript and prepared all the figures.

Competing interests

The authors declare that they have no conflict of interest.

Acknowledgements

The authors acknowledge funding from JSPS KAKENHI grant 17H06104 and MEXT KAKENHI grant 17H06323, and JAMSTEC for use of the Earth Simulator supercomputer.

https://doi.org/10.5194/cp-2020-17
Preprint. Discussion started: 19 February 2020
© Author(s) 2020. CC BY 4.0 License.

References

Bakker, P., Schmittner, A., Lenaerts, J.T.M., Abe-Ouchi, A., Bi, D., van den Broeke, M.R., Chan, W.-L., Hu, A., Beadling, R.L., Marsland, S.J., Mernild, S.H., Saenko, O.A., Swingedouw, D., Sullivan, A. and Yin, Y.: Fate of the Atlantic Meridional Overturning Circulation: Strong decline under continued warming and Greenland melting, Geophys. Res. Lett., 43, https://doi.org/10.1002/2016GL070457, 2016.

Bartoli, G., Hönisch, B. and Zeebe, R.E.: Atmospheric CO_2 decline during the Pliocene intensification of Northern Hemisphere glaciations, Paleoceanography, 26, PA4213, https://doi.org/10.1029/2010PA002055, 2011.

Braconnot P., Otto-Bliesner, B., Harrison, S., Joussaume, S., Peterchmitt, J.-Y., Abe-Ouchi, A., Crucifix, M., Driesschaert, E., Fichefet, Th., Hewitt, C.D., Kageyama, M., Kitoh, A., Laîné, A., Loutre, M.-F., Marti, O., Merkel, U., Ramstein, G., Valdes, P., Weber, S.L., Yu, Y. and Zhao, Y.: Results of PMIP2 coupled simulations of the Mid-Holocene and Last Glacial Maximum - Part 1: experiments and large-scale features, Clim. Past, 3, 261-277, https//doi.org/10.5194/cp-3-261-2007, 2007.

Brigham-Grette, J., Melles, M., Minyuk, P., Andreev, A., Tarasov, P., DeConto, R., Koenig, S., Nowaczyk, N., Wennrich, V., Rosén, P., Haltia, E., Cook, T., Gebhardt, C., Meyer-Jacob, C., Snyder, J. and Herzschuh, U.: Pliocene Warmth, Polar Amplification, and Stepped Pleistocene Cooling Recorded in NE Arctic Russia, Science, 340, 1421–1427, https://doi.org/10.1126/science.1233137, 2013.

Burke, K.D., Williams, J.W., Chandler, M.A., Haywood, A.M., Lunt, D.J. and Otto-Bliesner, B.L.: Pliocene and Eocene provide best analogs for near-future climates, Proc. Natl., Acad. Sci., 115, 13288-13293, https://doi.org/10.5061/dryad.0j18k00, 2018.

Chan, W.-L., Abe-Ouchi, A. and Ohgaito, R.: Simulating the mid-Pliocene climate with the MIROC general circulation model: experimental design and initial results, Geosci. Model Dev., 4, 1035–1049, https://doi.org/10.5194/gmd-4-1035-2011, 2011.

Chandan, D. and Peltier, W.R.: Regional and global climate for the mid-Pliocene using the University of Toronto version of CCSM4 and PlioMIP2 boundary conditions, Clim. Past, 13, 919-942, https://doi.org/10.5194/cp-13-919-2017, 2017.

Chandler, M.A., Rind, D. and Thompson, R.: Joint investigations of the middle Pliocene II: GISS GCM Northern Hemisphere results, Global Planet. Change, 9, 197–219, https://doi.org/10.1016/0921-8181(94)90016-7, 1994.

Chandler, M., Dowsett, H. and Haywood, A.: The PRISM Model/Data Cooperative: Mid-Pliocene data–model comparisons, PAGES News, 16, 24–25, 2008.

Crampton-Flood, E.M., Peterse, F., Munsterman, D. and Sinninghe Damsté, J.S.: Using tetraether lipids archived in North Sea Basin sediments to extract North Western European Pliocene continental air temperatures, Earth Planet. Sci. Lett., 490, 193-205, https://doi.org/10.1016/j.epsl.2018.03.030, 2018.

Dolan, A.M., Haywood, A.M., Hill, D.J., Dowsett, H.J., Hunter, S.J., Lunt, D.J. and Pickering, S.J.: Sensitivity of Pliocene ice sheets to orbital forcing, Palaeogeo. Palaeoclim. Palaeocol., 309, 98-110, https://doi.org/10.1016/j.palaeo.2011.03.030, 2011.

https://doi.org/10.5194/cp-2020-17
Preprint. Discussion started: 19 February 2020
© Author(s) 2020. CC BY 4.0 License.

Dowsett, H., Thompson, R., Barron, J., Cronin, T., Fleming, F., Ishman, S., Poore, R., Willard, D. and Holtz Jr., T.: Joint investigations of the Middle Pliocene climate I: PRISM paleoenvironmental reconstructions, Glob. Planet. Change, 9, 169-195, https://doi.org/10.1016/0921-8181(94)90015-9, 1994.

Dowsett, H. J., Barron, J. A., Poore, R. Z., Thompson, R. S., Cronin, T. M., Ishman, S. E., and Willard, D. A.: Middle Pliocene paleoenvironmental reconstruction: PRISM2, US Geol. Surv., Open File Rep., 99–535, 1999.

Dowsett, H., Dolan, A., Rowley, D., Moucha, R., Forte, A.M., Mitrovica, J.X., Pound, M., Salzmann, U., Robinson, M., Chandler, M., Foley, K., and Haywood, A.: The PRISM4 (mid-Piacenzian) paleoenvironmental reconstruction, Clim. Past, 12, 1519-1538, https://doi.org/10.5194/cp-12-1519-2016, 2016.

Dowsett, H.J., Foley, K.M., Stoll, D.K., Chandler, M.A., Sohl, L.E., Bentsen, M., Otto-Bliesner, B.L., Bragg, F.J., Chan, W.-L., Contoux, C., Dolan, A.M., Haywood, A.M., Jonas, J.A., Jost, A., Kamae, Y., Lohmann, G., Lunt, D.J., Nisancioglu, K.H., Abe-Ouchi, A., Ramstein, G., Riesselman, C.R., Robinson, M.M., Rosenbloom, N.A., Salzmann, U., Stepanek, C., Strother, S.L., Ueda, H., Yan, Q. and Zhang, Z.: Sea Surface Temperature of the mid-Piacenzian Ocean: A Data-Model Comparison. Scientific Reports, 3, https://doi.org/10.1038/srep02013, 2013.

Fedorov, A.V., Brierley, C.M., Lawrence, K.T., Liu, Z., Dekens, P.S. and Ravelo, A.C.: Patterns and mechanisms of early Pliocene warmth, Nature, 496, 43-49, https://doi.org/10.1038/nature12003, 2013.

Foley, K.M. and Dowsett, H.J.: Community sourced mid-Piacenzian sea surface temperature (SST) data: US Geological Survey data release: https://doi.org/10.5066/P9YP3DTV, 2019.

Haywood, A.M., Dowsett, H.J., Otto-Bliesner, B., Chandler, M.A., Dolan, A.M., Hill, D.J., Lunt, D.J., Robinson, M.M., Rosenbloom, N., Salzmann, U., and Sohl, L.E.: Pliocene Model Intercomparison Project (PlioMIP): experimental design and boundary conditions (Experiment 1), Geosci. Model Dev., 3, 227–242, https://doi.org/10.5194/gmd-3-227-2010, 2010.

Haywood, A.M., Dowsett, H.J., Robinson, M.M., Stoll, D.K., Dolan, A.M., Lunt, D.J., Otto-Bliesner, B., and Chandler, M.A.: Pliocene Model Intercomparison Project (PlioMIP): experimental design and boundary conditions (Experiment 2), Geosci. Model Dev., 4, 571–577, https://doi.org/10.5194/gmd-4-571-2011, 2011.

Haywood, A.M., Dowsett, H.J., Dolan, A.M., Rowley, D., Abe-Ouchi, A., Otto Bliesner, B., Chandler, M.A., Hunter, S.J., Lunt, D.J., Pound, M. and Salzmann, U.: The Pliocene Model Intercomparison Project (PlioMIP) Phase 2: scientific objectives and experimental design, Clim. Past, 12, 663-675, https://doi.org/10.5194/cp-12-663-2016, 2016.

Haywood, A.M., Hill, D.J., Dolan, A.M., Otto-Bliesner, B.L., Bragg, F., Chan, W.-L., Chandler, M.A., Contoux, C., Dowsett, H.J., Jost, A., Kamae, Y., Lohmann, G., Lunt, D.J., Abe-Ouchi A., Pickering, S.J., Ramstein, G., Rosenbloom, N.A., Salzmann, U., Sohl, L., Stepanek, C., Ueda, H., Yan, Q. and Zhang, Z.: Large-scale features of Pliocene climate: results from the Pliocene Model Intercomparison Project, Clim. Past, 9, 191–209, https://doi.org/10.5194/cp-9-191-2013, 2013.

Haywood, A.M., Tindall, J.C., Dowsett, H.J., Dolan, A.M., Foley, K.M., Hunter, S.J., Hill, D.J., Chan, W.-L., Abe-Ouchi, A., Stepanek, C., Lohmann, G., Chandan, D., Peltier, W.R., Tan, N., Contoux, C., Ramstein, G., Li, X., Zhang, Z., Guo, C., Nisancioglu, K.H., Zhang, Q., Li, Q., Kamae, Y., Chandler, M.A., Sohl, L.E., Otto-Bliesner, B.L., Feng, R., Brady, E.C., von

© Author(s) 2020. CC BY 4.0 License.


der Heydt, A.S., Baatsen, M.L.J., and Lunt, D.J.: A return to large-scale features of Pliocene climate: the Pliocene Model Intercomparison Project Phase 2, Clim. Past Discuss., https://doi.org/10.5194/cp-2019-145, in review, 2020.

Haywood, A.M. and Valdes, P.J.: Modelling Pliocene warmth: contribution of atmosphere, oceans and cryosphere, Earth Planet. Sci. Lett., 218, 363-377, https://doi.org/10.1016/S0012-821X(03)00685-X, 2004.

Hill, D.J., Haywood, A.M., Lunt, D.J., Hunter, S.J., Bragg, F.J., Contoux, C., Stepanek, C., Sohl, L., Rosenbloom, N.A., Chan, W.L., Kamae, Y., Zhang, Z., Abe Ouchi, A., Chandler, M.A., Jost, A., Lohmann, G., Otto Bliesner, B.L., Ramstein, G., and Ueda, H.: Evaluating the dominant components of warming in Pliocene climate simulations, Clim. Past, 10, 79-90, https://doi.org/10.5194/cp-10-79-2014, 2014.

Hunter, S.J., Haywood, A.M., Dolan, A.M. and Tindall, J.C.: The HadCM3 contribution to PlioMIP Phase 2, Clim. Past, 15, 1691–1713, https://doi.org/10.5194/cp-15-1691-2019, 2019.

IPCC: Climate Change 2013: The Physical Science Basis. Contribution of Working Group I of the Fifth Assessment Report of the Intergovernmental Panel on Climate Change, edited by Stocker, T.F., Qin, D., Plattner, G.-K., Tignor, M., Allen, S.K., Boschung, J., Nauels, A., Xia, Y., Bex, V. and Midgley, P.M., Cambridge University Press, 1585pp., 2013.

Jochum, M., Fox-Kemper, B., Molnar, P.H. and Shields, C.: Differences in the Indonesian seaway in a coupled climate model and their relevance to Pliocene climate and El Niño, Paleoceanography, 24, PA1212, https://doi.org/10.1029/2008PA001678, 2009.

K-1 model developers: K-1 coupled model (MIROC) description. K-1 technical report, edited by: Hasumi, H. and Emori, S., Center for Climate System Research, The University of Tokyo, Japan, 34 pp., 2004.

Hasumi, H.: CCSR Ocean Component Model (COCO) Version 2.1, CCSR Report, The University of Tokyo, Japan, 13, 68 pp., 2000.

Kageyama, M., Braconnot, P., Harrison, S.P., Haywood, A.M., Jungclaus, J.H., Otto-Bliesner, B.L., Peterschmitt, J.-Y., Abe-Ouchi, A., Albani, S., Bartlein, P.J., Brierley, C., Crucifix, M., Dolan, A., Fernandez-Donado, L., Fischer, H., Hopcroft, P.O., Ivanovic, R.F., Lambert, F., Lunt, D.J., Mahowald, N.M., Peltier, W.R., Phipps, S.J., Roche, D.M., Schmidt, G.A., Tarasov, L., Valdes, P.J., Zhang, Q. and Zhou, T.: The PMIP4 contribution to CMIP6 - Part 1: Overview and over-arching analysis plan, Geosci. Model Dev., 11, 1033–1057, https://doi.org/10.5194/gmd-11-1033-2018, 2018.

Kürschner, W.M., van der Burgh, J., Visscher, H. and Dilcher, D.L.: Oak leaves as biosensors of late Neogene and early Pleistocene paleoatmospheric CO_2 concentrations, Mar. Micropaleontol., 27, 299–312, https://doi.org/10.1016/0377-8398(95)00067-4, 1996.

Li, X., Guo, C., Zhang, Z., Otterå, O.H. and Zhang, R.: PlioMIP2 simulations with NorESM-L and NorESM1-F, Clim. Past, 16, 183-197, https://doi.org/10.5194/cp-16-183-2020, 2020.

Lunt, D.J., Haywood, A.M., Schmidt, G.A., Salzmann, U., Valdes, P.J. and Dowsett, H.J.: Earth system sensitivity inferred from Pliocene modelling and data, Nature Geosci., 3, 60-64, https://doi.org/10.1038/NGEO706, 2010.

Lunt, D.J., Valdes, P.J., Haywood, A.M. and Rutt, I.C.: Closure of the Panama Seaway during the Pliocene: implications for climate and Northern Hemisphere glaciation, Clim. Dyn., 30, 1-18, https://doi.org/10.1007/s00382-007-0265-6, 2008.

© Author(s) 2020. CC BY 4.0 License.

Noh, Y. and Kim, H.-J.: Simulations of temperature and turbulence structure of the oceanic boundary layer with the improved near-surface process, J. Geophys. Res., 104, 15621–15634, https://doi.org/10.1029/1999JC900068, 1999.

Numaguti, A., Takahashi, M., Nakajima, T., and Sumi, A.: Description of CCSR/NIES Atmospheric General Circulation Model, CGERs Supercomputer Monograph Report, Center for Global Environment Research, National Institute for Environmental Studies, 3, 1–48, 1997.

Obase, T. and Abe-Ouchi, A.: Abrupt Bølling-Allerød Warming Simulated under Gradual Forcing of the Last Deglaciation, Geophys. Res. Lett., 46, 11397-11405, https://doi.org/10.1029/2019GL084675, 2019.

Ohgaito, R. Sueyoshi, T., Abe-Ouchi, A., Hajima, T., Watanabe, S., Kim, H.-J., Yamamoto, A. and Kawamiya, M.: Can an Earth System Model simulate better climate change at mid-Holocene than an AOGCM? A comparison study of MIROC-ESM and MIROC3, Clim. Past, 9, 1519–1542, https://doi.org/10.5194/cp-9-1519-2013, 2013.

O'ishi, R. and Abe-Ouchi, A: Polar amplification in the mid-Holocene derived from dynamical vegetation change with a GCM, Geophys. Res. Lett., 38, L14702, https://doi.org/10.1029/2011GL048001, 2011.

O'ishi, R. and Abe-Ouchi, A.: Influence of dynamic vegetation on climate change and terrestrial carbon storage in the Last Glacial Maximum, Clim. Past, 9, 1571-1587, https://doi.org/10.5194/cp-9-1571-2013, 2013.

Oka, A., Hasumi, H., Okada, N., Sakamoto, T.T. and Suzuki, T.: Deep convection seesaw controlled by freshwater transport through the Denmark Strait, Ocean Modell., 15, 157-176, https://doi.org/10.1016/j.ocemod.2006.08.004, 2006.

Otto-Bliesner, B.L., Jahn, A. Feng, R. Brady, E.C., Hu, A. and Löfverström, M.: Amplified North Atlantic warming in the late Pliocene by changes in Arctic gateways, Geophys. Res. Lett., 44, 957–964, https://doi.org/10.1002/2016GL071805, 2017.

Prescott, C.L., Dolan, A.M., Haywood, A.M., Hunter, S.J. and Tindall, J.C.: Regional climate and vegetation response to orbital forcing within the mid-Pliocene Warm Period: A study using HadCM3, Glob. Planet. Change, 161, 231-243, https://doi.org/10.1016/j.gloplacha.2017.12.015, 2018.

Raymo, M., Grant, B., Horowitz, M. and Rau, G.: Mid-Pliocene warmth: stronger greenhouse and stronger conveyor, Mar. Micropaleontol. 27, 313–326, https://doi.org/10.1016/0377-8398(95)00048-8, 1996.

Salzmann, U., Haywood, A. M., Lunt D. J., Valdes, P. J., and Hill, D. J.: A new global biome reconstruction and data-model comparison for the Middle Pliocene, Global Ecol. Biogeogr., 17, 432–447, https://doi.org/10.1111/j.1466-8238.2008.00381.x, 2008.

Sherriff-Tadano, S. and Abe-Ouchi, A.: Roles of sea ice-surface wind feedback in maintaining the glacial Atlantic meridional overturning circulation and climate, J. Clim., https://doi.org/10.1175/JCLI-D-19-0431.1, in press, 2020.

Takata, K., Watanabe, T., and Emori, S.: Development of the minimal advanced treatments of surface interaction and runoff, Global Planet. Change, 38, 209–222, https://doi.org/10.1016/S0921-8181(03)00030-4, 2003.

Seki, O., Foster, G.L., Schmidt, D.N., Mackensen, A., Kawamura, K. and Pancost, R.D.: Alkenone and boron-based Pliocene pCO_2 records, Earth Planet. Sci. Lett. 292, 201–211, https://doi.org/10.1016/j.epsl.2010.01.037, 2010.

Sloan, L.C., Crowley, T.J. and Pollard, D.: Modeling of middle Pliocene climate with the NCAR GENESIS general circulation model, Mar. Micropaleontol., 27, 51–61, https://doi.org/10.1016/0377-8398(95)00063-1, 1996.

© Author(s) 2020. CC BY 4.0 License.

Sévellec, F. and Fedorov, A.V.: AMOC sensitivity to surface buoyancy fluxes: Stronger ocean meridional heat transport with a weaker volume transport?, Clim. Dyn., 47, https://doi.org/10.1007/s00382-015-2915-4, 1497-1513, 2016.

Takemura, T., Okamoto, H., Maruyama, Y., Numaguti, A., Higurashi, A., and Nakajima, T.: Global three-dimensional simulation of aerosol optical thickness distribution of various origins, J. Geophys. Res., 105, 17853–17873, https://doi.org/10.1029/2000JD900265, 2000.

Tan, N., Contoux, C., Ramstein, G., Sun, Y., Dumas, C., Sepulchre, P. and Guo, Z.: Modeling a modern-like pCO2 warm period (Marine Isotope Stage KM5c) with two versions of an Institut Pierre Simon Laplace atmosphere–ocean coupled general circulation model, Clim. Past, 16, 1-16, https://doi.org/10.5194/cp-16-1-2020, 2020.

Tripati, A.K., Roberts, C.D. and Eagle, R.A.: Coupling of CO_2 and ice sheet stability over major climate transitions of the last 20 million years, Science, 326, 1394–1397, https://doi.org/10.1126/science.1178296, 2009.

Willeit, M., Ganopolski, A. and Feulner, G.: On the effect of orbital forcing on mid-Pliocene climate, vegetation and ice sheets, Clim. Past, 9, 1749-1759, https://doi.org/10.5194/cp-9-1749-2013, 2013.

Yanase, W. and Abe-Ouchi, A.: The LGM surface climate and atmospheric circulation over East Asia and the North Pacific in the PMIP2 coupled model simulations, Clim. Past, 3, 439–451, https://doi.org/10.5194/cp-3-439-2007, 2007.

Zhang, R., Yan, Q., Zhang, Z.S., Jiang, D., Otto-Bliesner, B.L., Haywood, A.M., Hill, D.J., Dolan, A.M., Stepanek, C., Lohmann, G., Contoux, C., Bragg, F., Chan, W.L., Chandler, M.A., Jost, A., Kamae, Y., Abe-Ouchi, A., Ramstein, G., Rosenbloom, N.A., Sohl , L. and Ueda, H.: Mid-Pliocene East Asian monsoon climate simulated in the PlioMIP, Clim. Past, 9, 2085-2099, https://doi.org/10.5194/cp-9-2085-2013, 2013.

Zhang, Z.S., Nisancioglu, K.H., Chandler, M.A., Haywood, A.M., Otto-Bliesner, B.L., Ramstein, G., Stepanek, C., Abe-Ouchi, A., Chan, W.L., Bragg, F.J., Contoux , C., Dolan, A.M., Hill, D.J., Jost, A., Kamae, Y., Lohmann, G., Lunt, D.J., Rosenbloom, N.A., Sohl, L.E., and Ueda, H.: Mid-pliocene Atlantic Meridional Overturning Circulation not unlike modern, Clim. Past, 9, 1495-1504, https://doi.org/10.5194/cp-9-1495-2013, 2013.

https://doi.org/10.5194/cp-2020-17
Preprint. Discussion started: 19 February 2020
© Author(s) 2020. CC BY 4.0 License.

Climate of the Past Discussions
Open Access
EGU

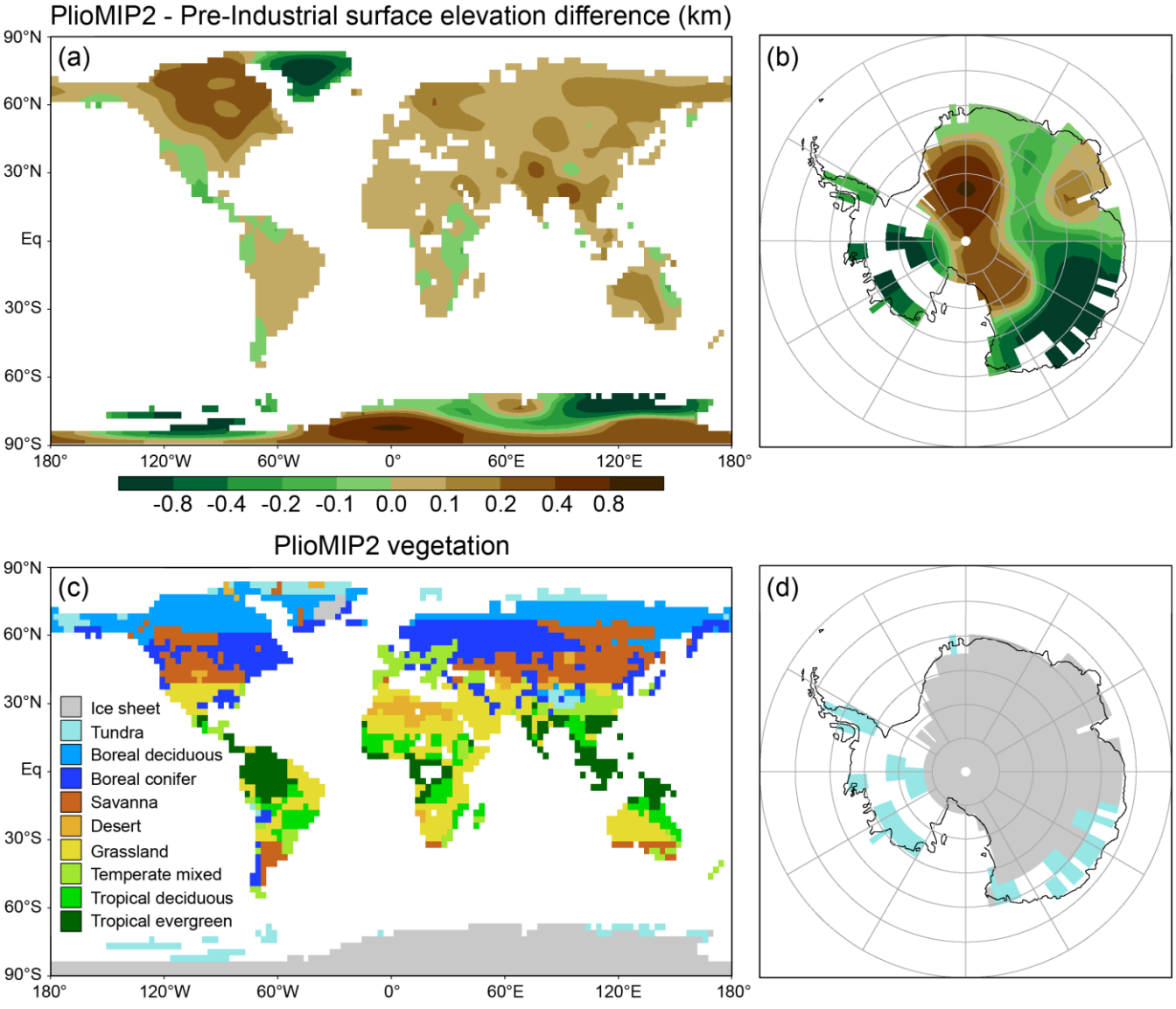

Figure 1: (a) The difference between land elevation in the Pliocene and present day experiments, and (b) the vegetation specified for Pliocene experiments on the MIROC4m grid.

https://doi.org/10.5194/cp-2020-17
Preprint. Discussion started: 19 February 2020
© Author(s) 2020. CC BY 4.0 License.

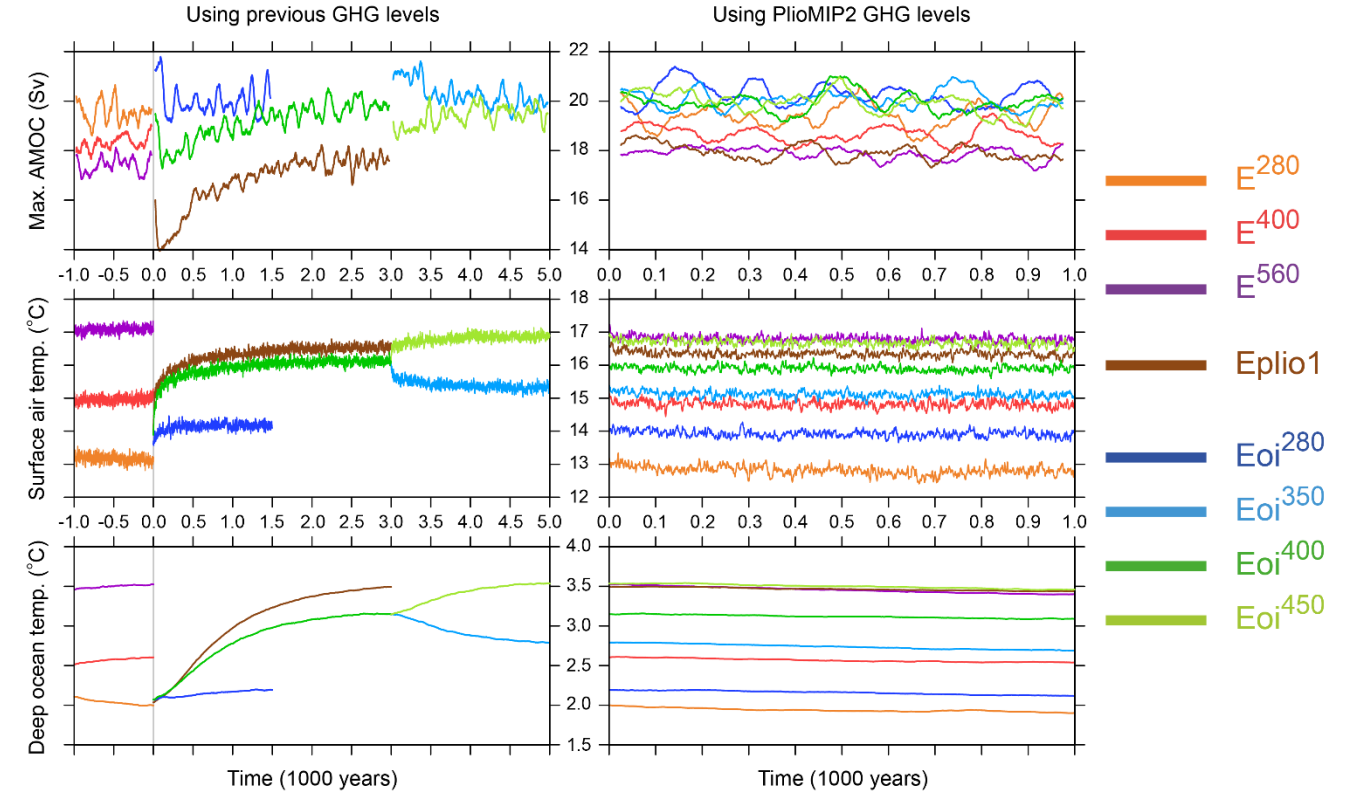

570 **Figure 2: Time series of the AMOC index (top), globally averaged surface air temperature (middle) and global ocean temperature below depths of 1900m (bottom). A 51-year moving average has been applied to the AMOC index time series. The subfigures on the left depict the initial stages of the experiments during which greenhouse gas levels are set to previous, PlioMIP1 values, while the subfigures on the right depict the final 1000 years of the integration during which greenhouse gas levels are consistent with those specified in PlioMIP2.**

https://doi.org/10.5194/cp-2020-17
Preprint. Discussion started: 19 February 2020
© Author(s) 2020. CC BY 4.0 License.

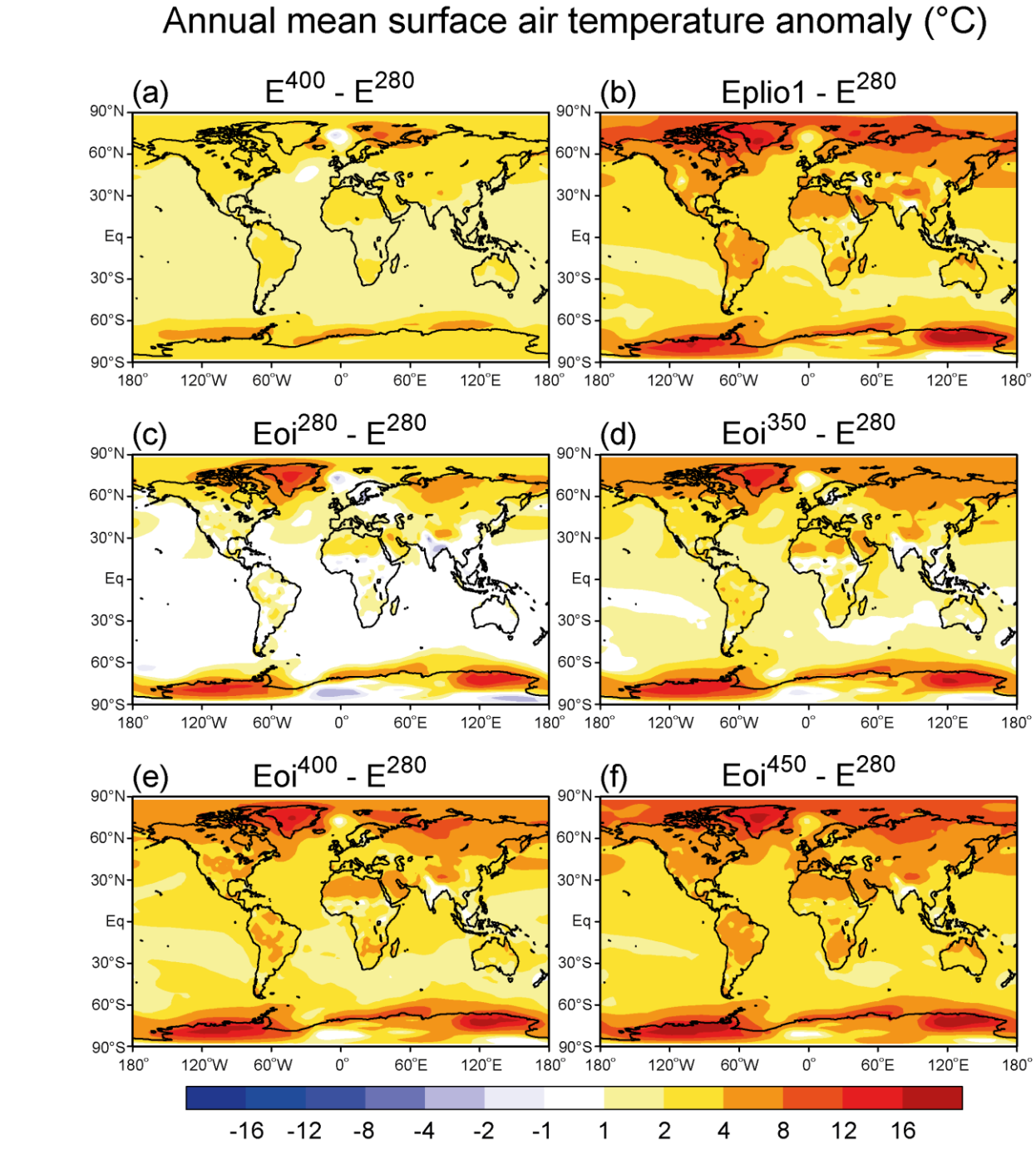

575

Figure 3: Annual mean surface air temperature anomaly between six experiments and E^{280}, the Pre-Industrial. For a comparison of PlioMIP1 and PlioMIP2, see (b) and (e). For the individual effects of CO_2 and Pliocene boundary conditions, see (a) and (c), respectively.

https://doi.org/10.5194/cp-2020-17
Preprint. Discussion started: 19 February 2020
© Author(s) 2020. CC BY 4.0 License.

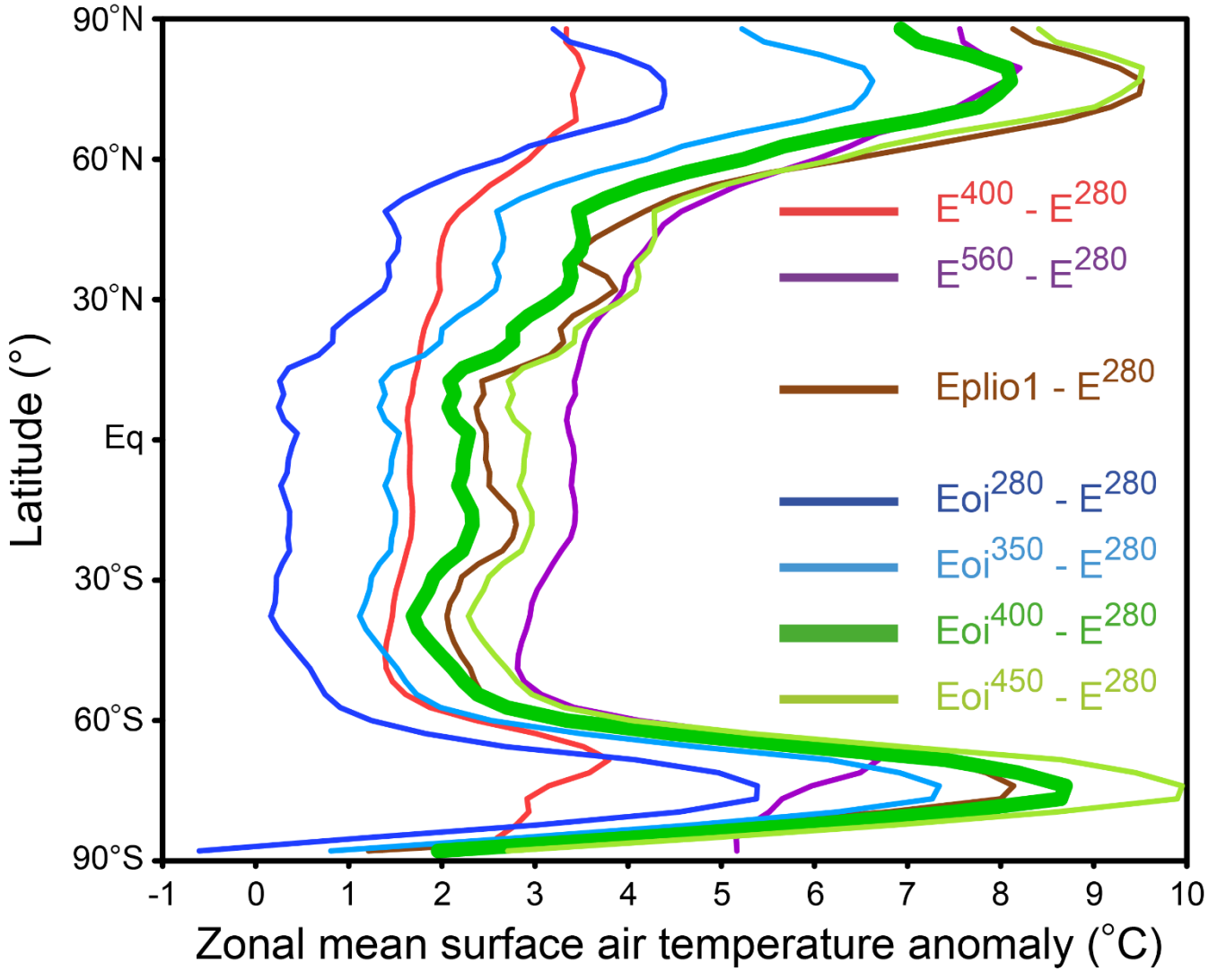

580 **Figure 4: Zonal mean surface air temperature anomaly. The core experiment, Eoi^{400}, is shown in bold green.**

https://doi.org/10.5194/cp-2020-17
Preprint. Discussion started: 19 February 2020
© Author(s) 2020. CC BY 4.0 License.

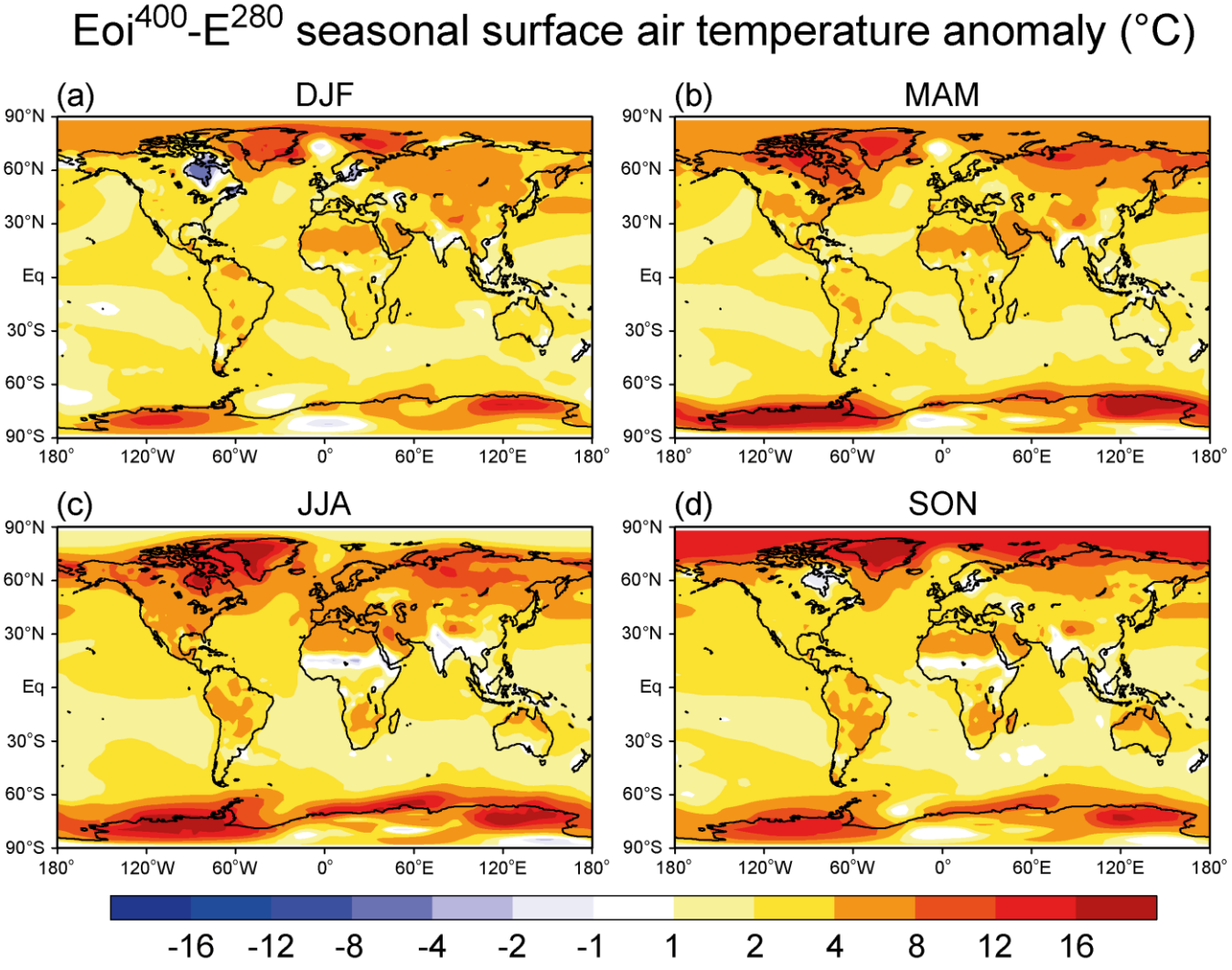

Figure 5: Seasonal surface air temperature anomaly between Eoi^{400} and E^{280} for December-February (DJF), March-May (MAM), June-August (JJA) and September-November (SON).

https://doi.org/10.5194/cp-2020-17
Preprint. Discussion started: 19 February 2020
© Author(s) 2020. CC BY 4.0 License.

Climate of the Past Discussions
Open Access
EGU

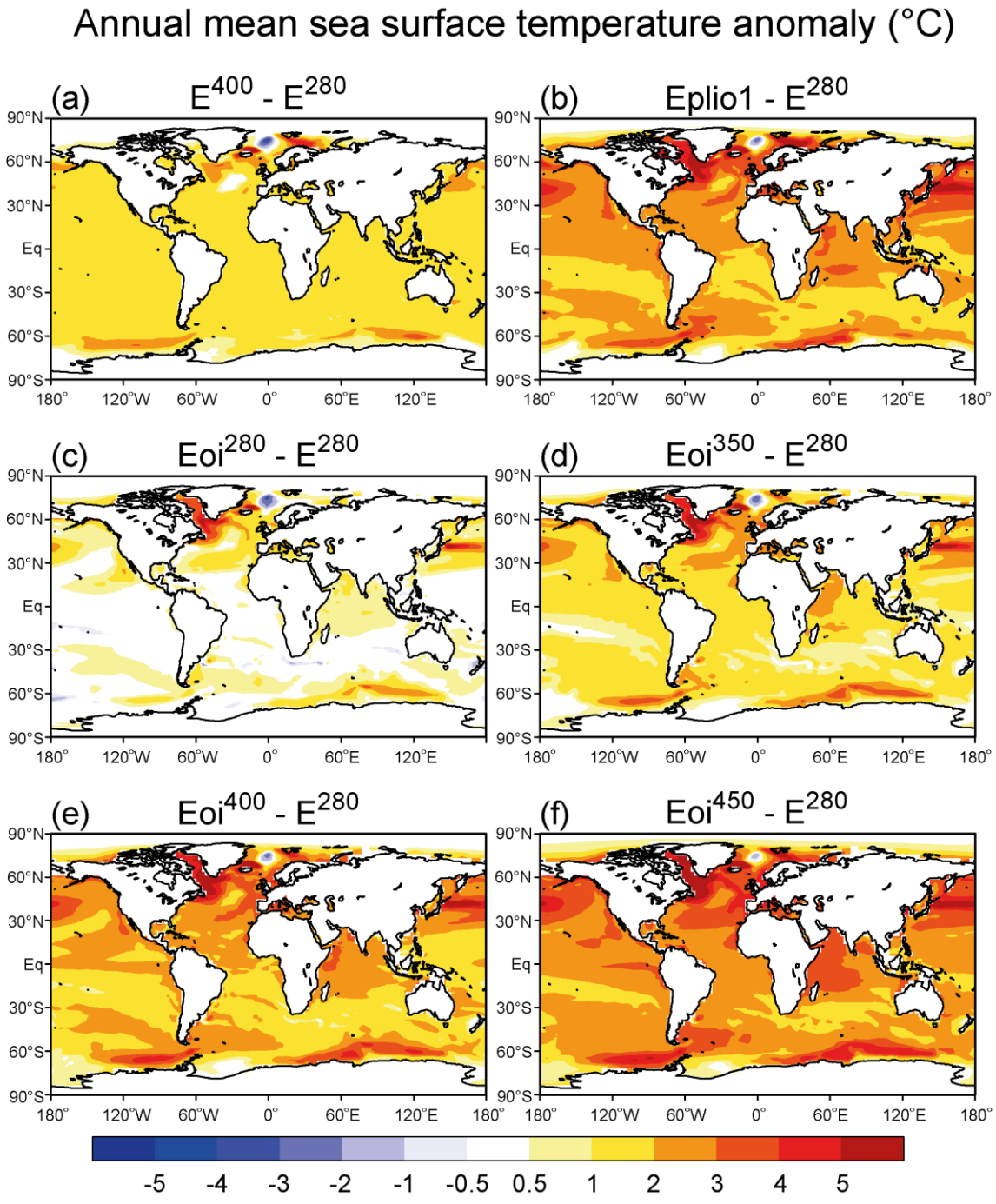

585 **Figure 6: Annual mean sea surface temperature anomaly between six experiments and E^{280}, the Pre-Industrial. For a comparison of PlioMIP1 and PlioMIP2, see (b) and (e). For the individual effects of CO_2 and Pliocene boundary conditions, see (a) and (c), respectively.**

https://doi.org/10.5194/cp-2020-17
Preprint. Discussion started: 19 February 2020
© Author(s) 2020. CC BY 4.0 License.

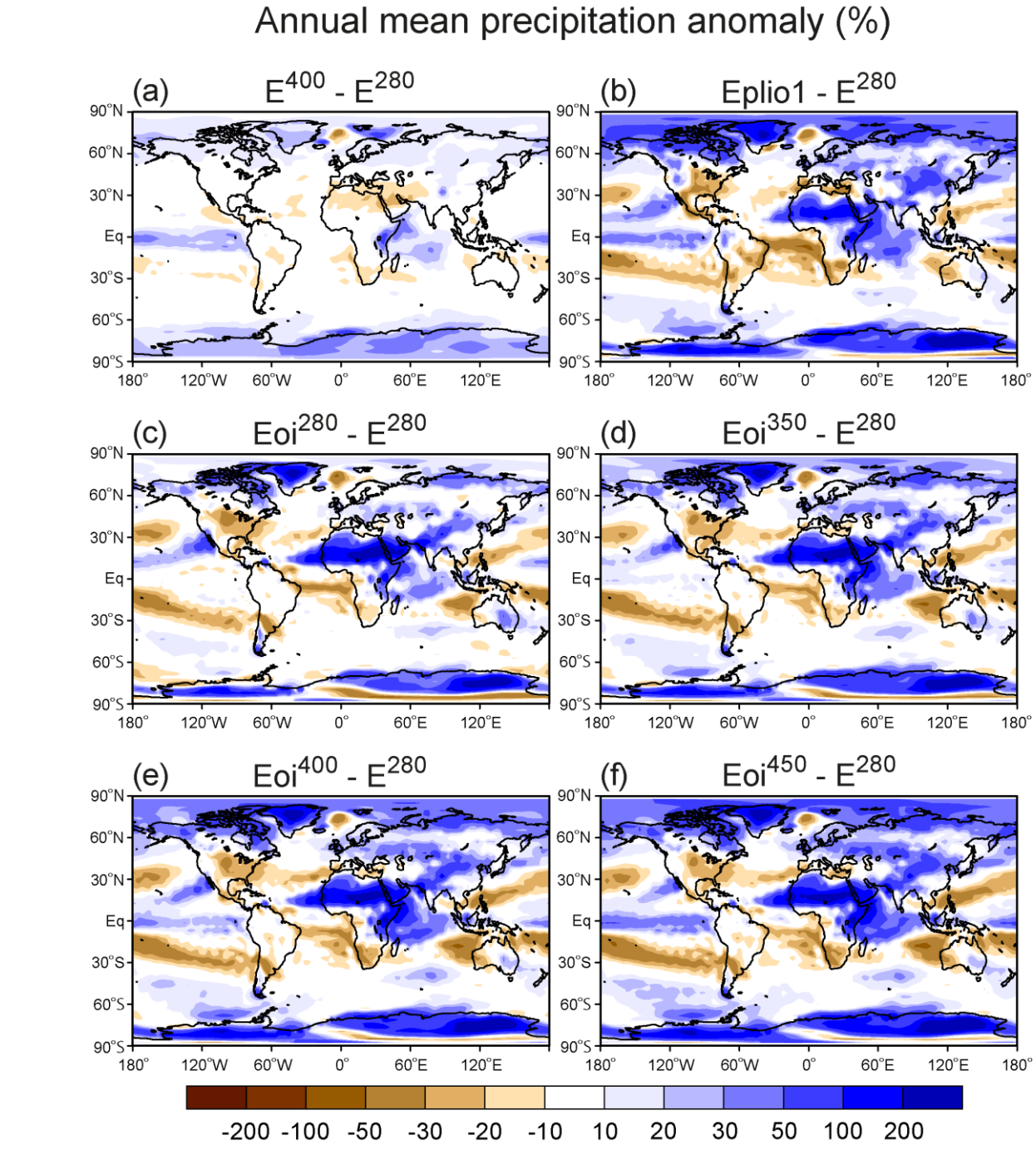

Figure 7: Annual mean precipitation anomaly between six experiments and E^{280}, the Pre-Industrial, as a percentage of E280, eg. 100 x (Eoi^{400} – E^{280}) / E^{280}. For a comparison of PlioMIP1 and PlioMIP2, see (b) and (e). For the individual effects of CO_2 and Pliocene boundary conditions, see (a) and (c), respectively.

https://doi.org/10.5194/cp-2020-17
Preprint. Discussion started: 19 February 2020
© Author(s) 2020. CC BY 4.0 License.

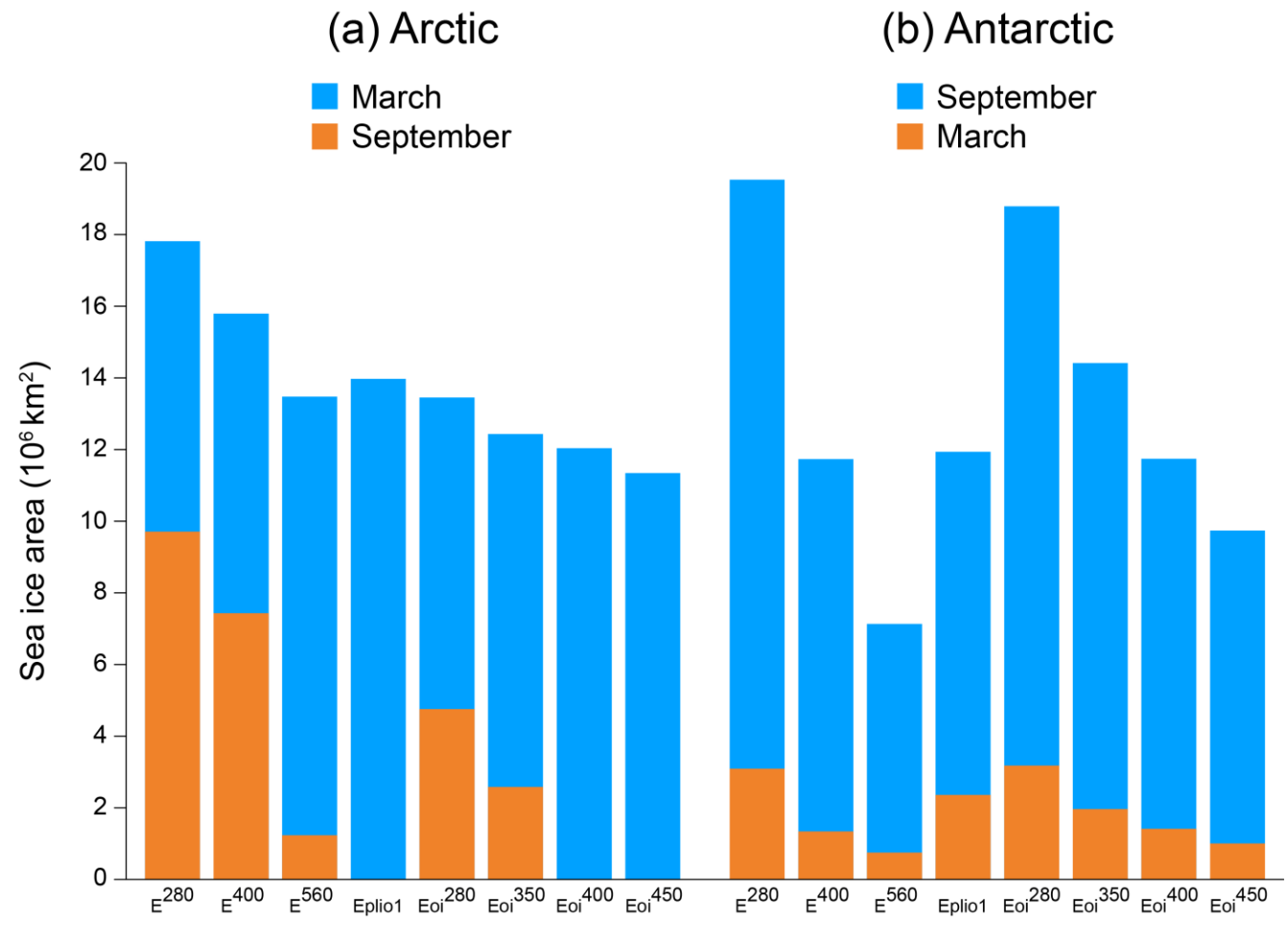

Figure 8: Total surface area of sea ice in each polar region during March and September.

https://doi.org/10.5194/cp-2020-17
Preprint. Discussion started: 19 February 2020
© Author(s) 2020. CC BY 4.0 License.

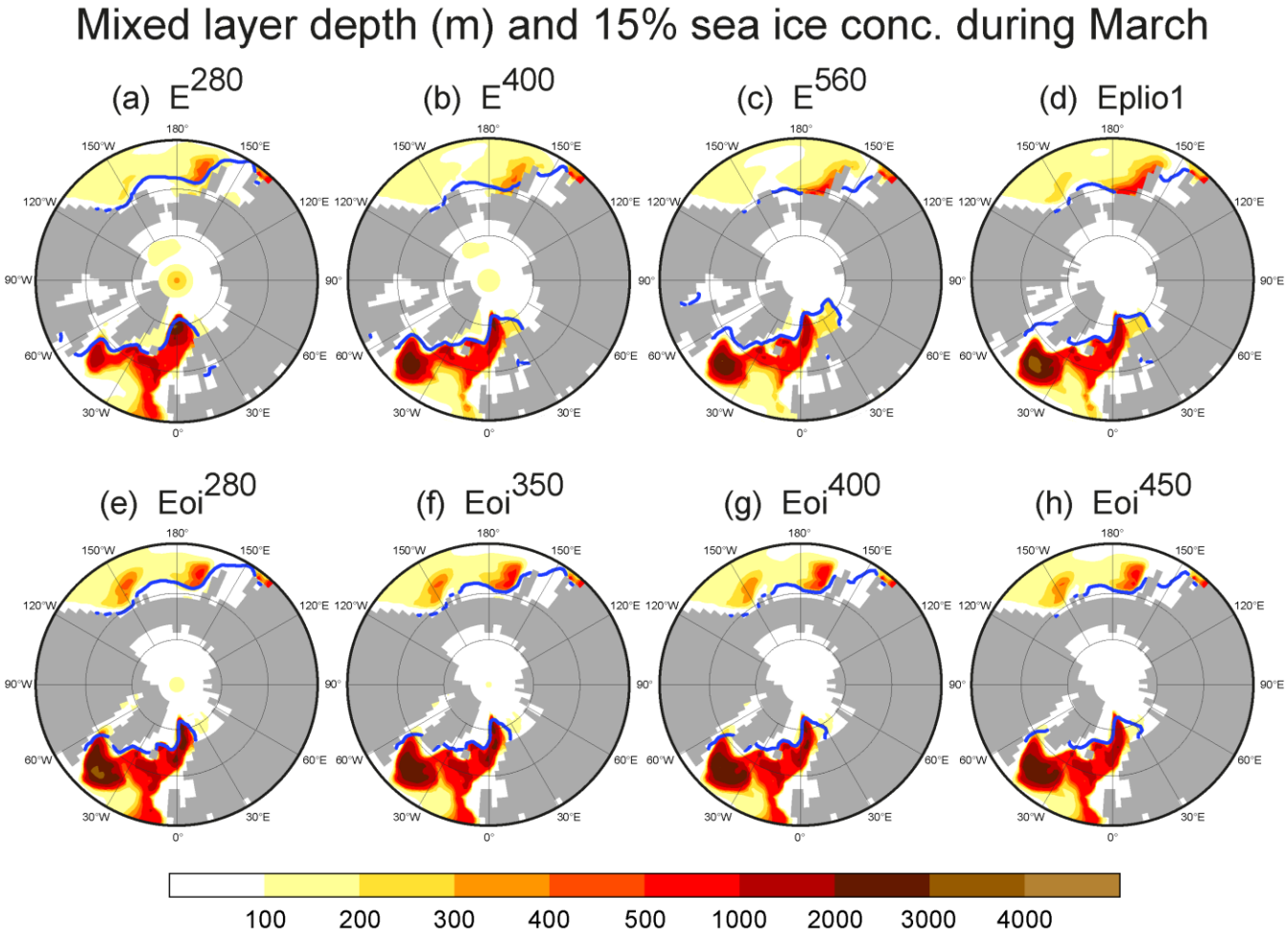

595

Figure 9: Oceanic mixed layer depth in the northern hemisphere during March. The blue lines indicate the extent of 15% sea ice concentration. For a comparison of PlioMIP1 and PlioMIP2, see (d) and (g). For the individual effects of CO_2 and Pliocene boundary conditions, see (b) and (e), respectively.

https://doi.org/10.5194/cp-2020-17
Preprint. Discussion started: 19 February 2020
© Author(s) 2020. CC BY 4.0 License.

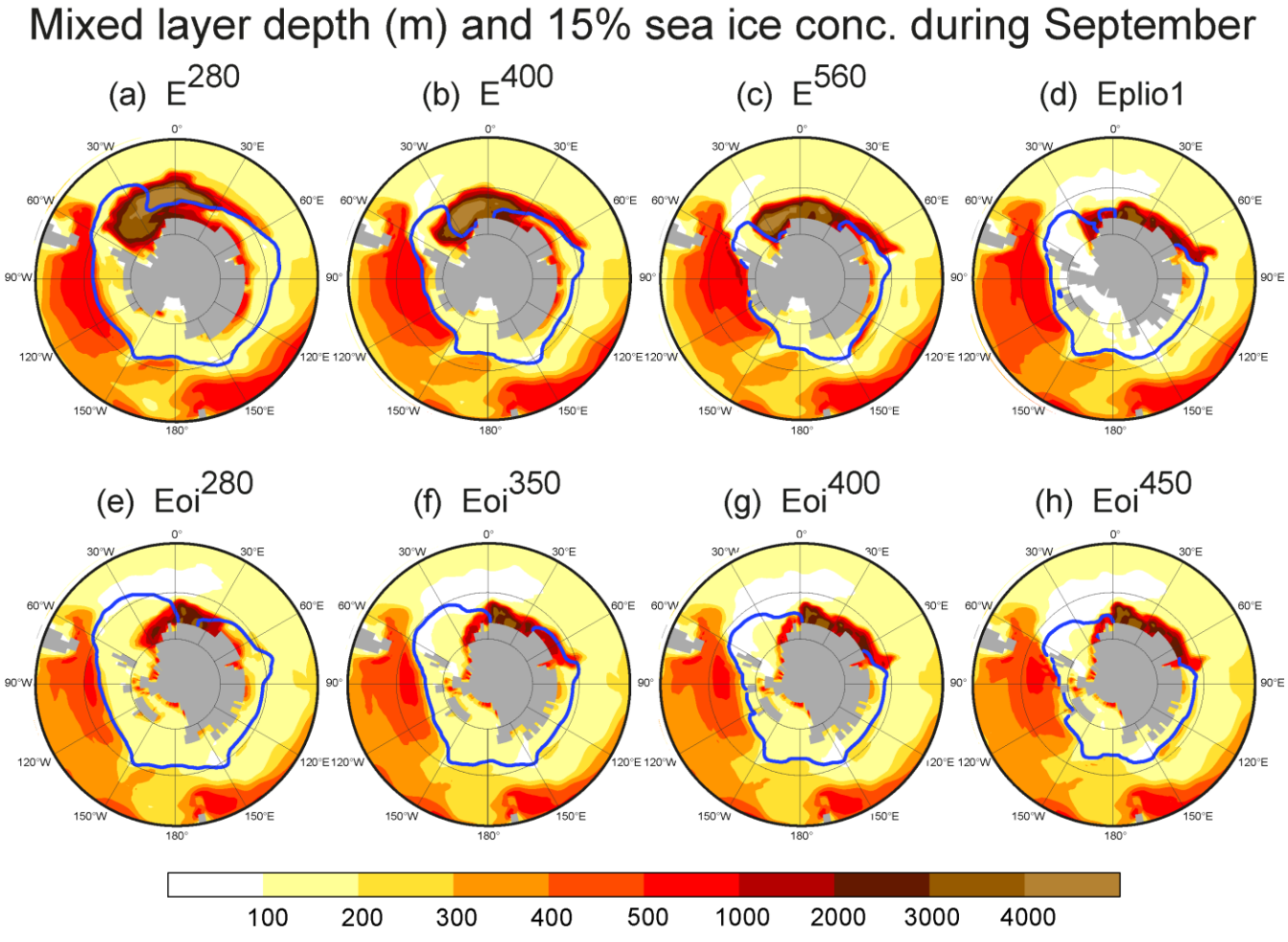

600

Figure 10: Oceanic mixed layer depth in the southern hemisphere during September. The blue lines indicate the extent of 15% sea ice concentration. For a comparison of PlioMIP1 and PlioMIP2, see (d) and (g). For the individual effects of CO_2 and Pliocene boundary conditions, see (b) and (e), respectively.

https://doi.org/10.5194/cp-2020-17
Preprint. Discussion started: 19 February 2020
© Author(s) 2020. CC BY 4.0 License.

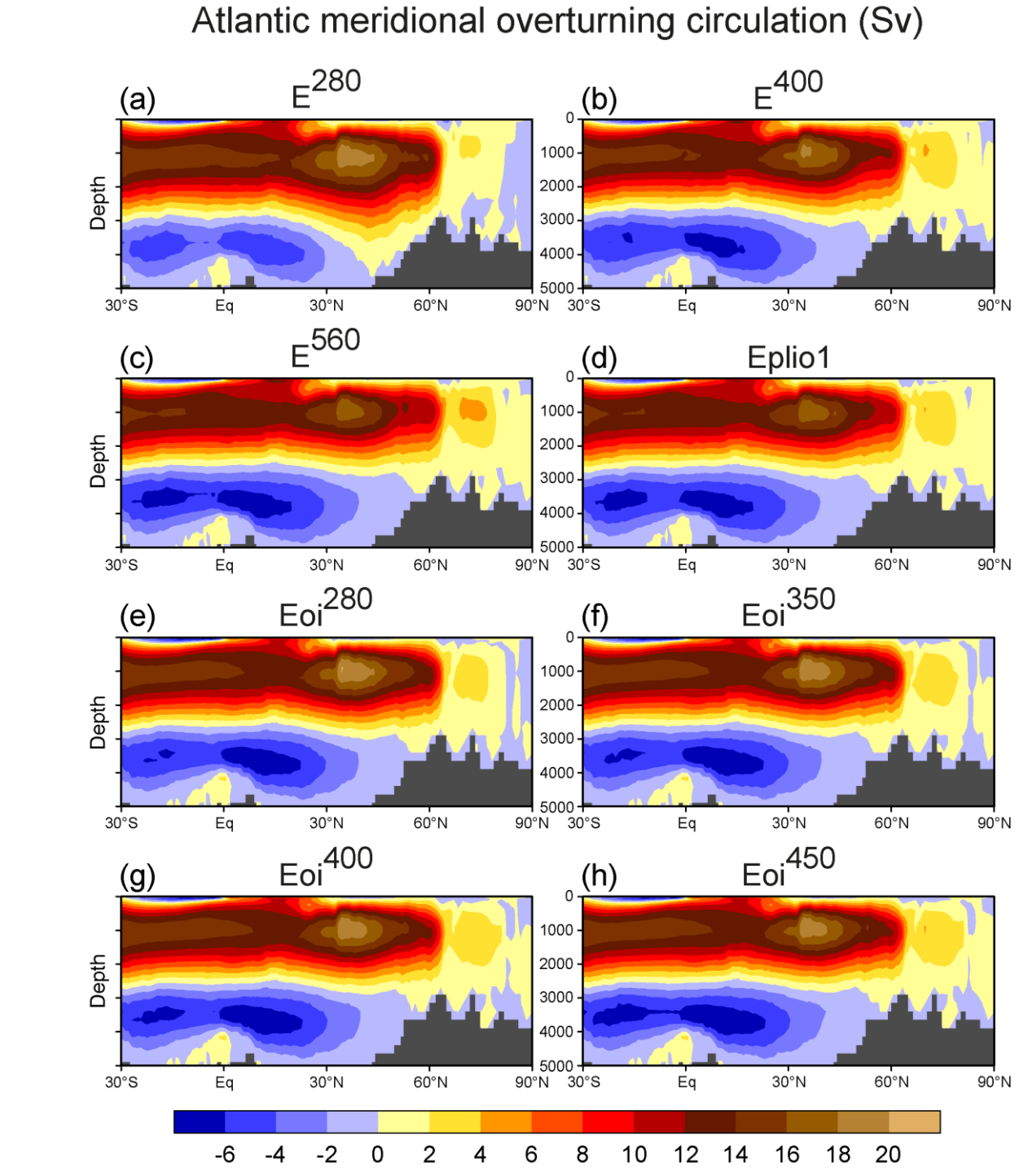

Figure 11: Streamfunction of the Atlantic meridional overturning circulation, averaged over the last 500 years. For a comparison of PlioMIP1 and PlioMIP2, see (d) and (g). For the individual effects of CO_2 and Pliocene boundary conditions, see (b) and (e), respectively.

https://doi.org/10.5194/cp-2020-17
Preprint. Discussion started: 19 February 2020
© Author(s) 2020. CC BY 4.0 License.

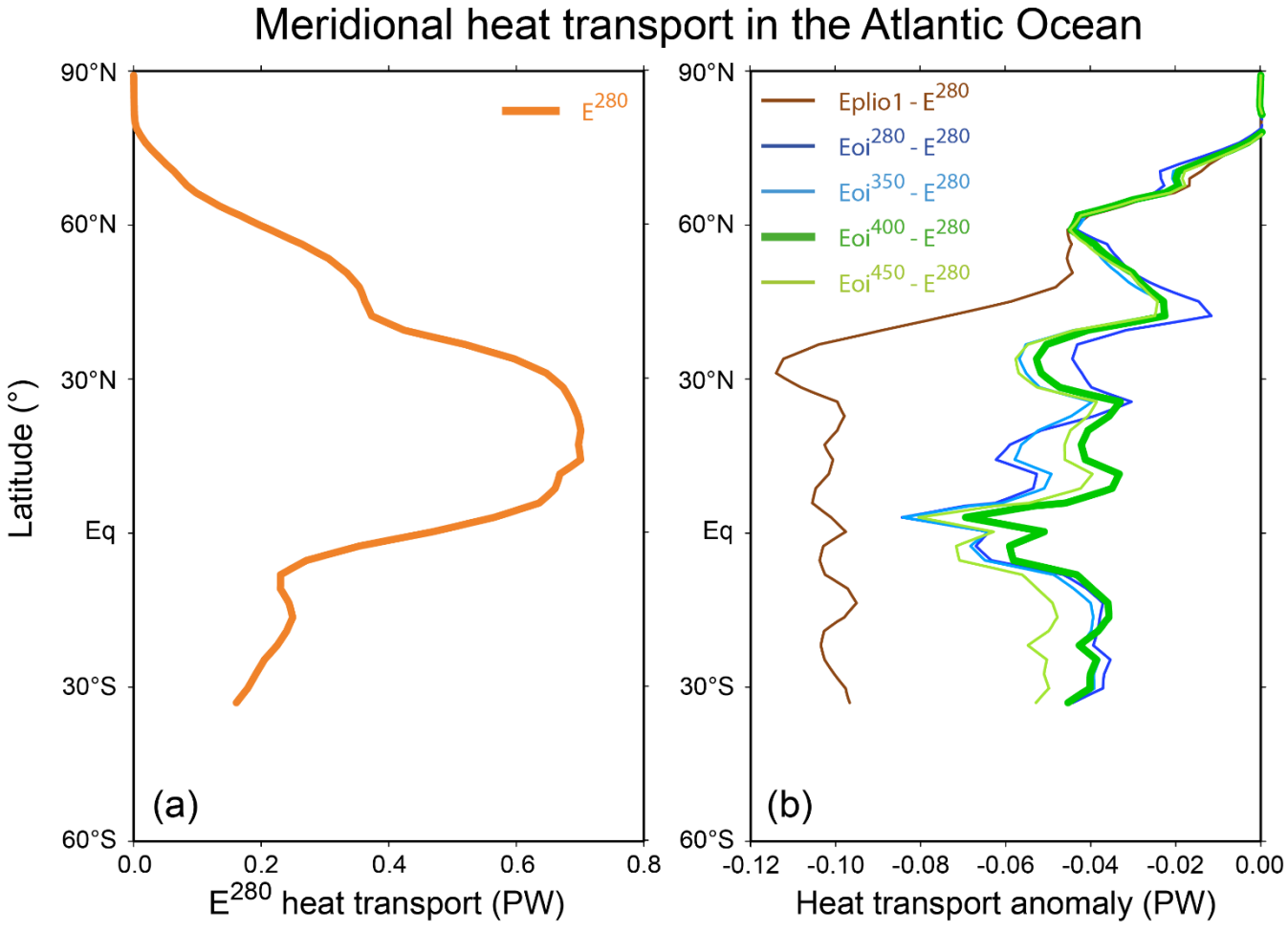

Figure 12: (a) The Atlantic Ocean meridional heat transport in E^{280} and (b) the anomaly between the Pliocene experiments and E^{280}. The core experiment, Eoi400, is shown in bold green.

https://doi.org/10.5194/cp-2020-17
Preprint. Discussion started: 19 February 2020
© Author(s) 2020. CC BY 4.0 License.

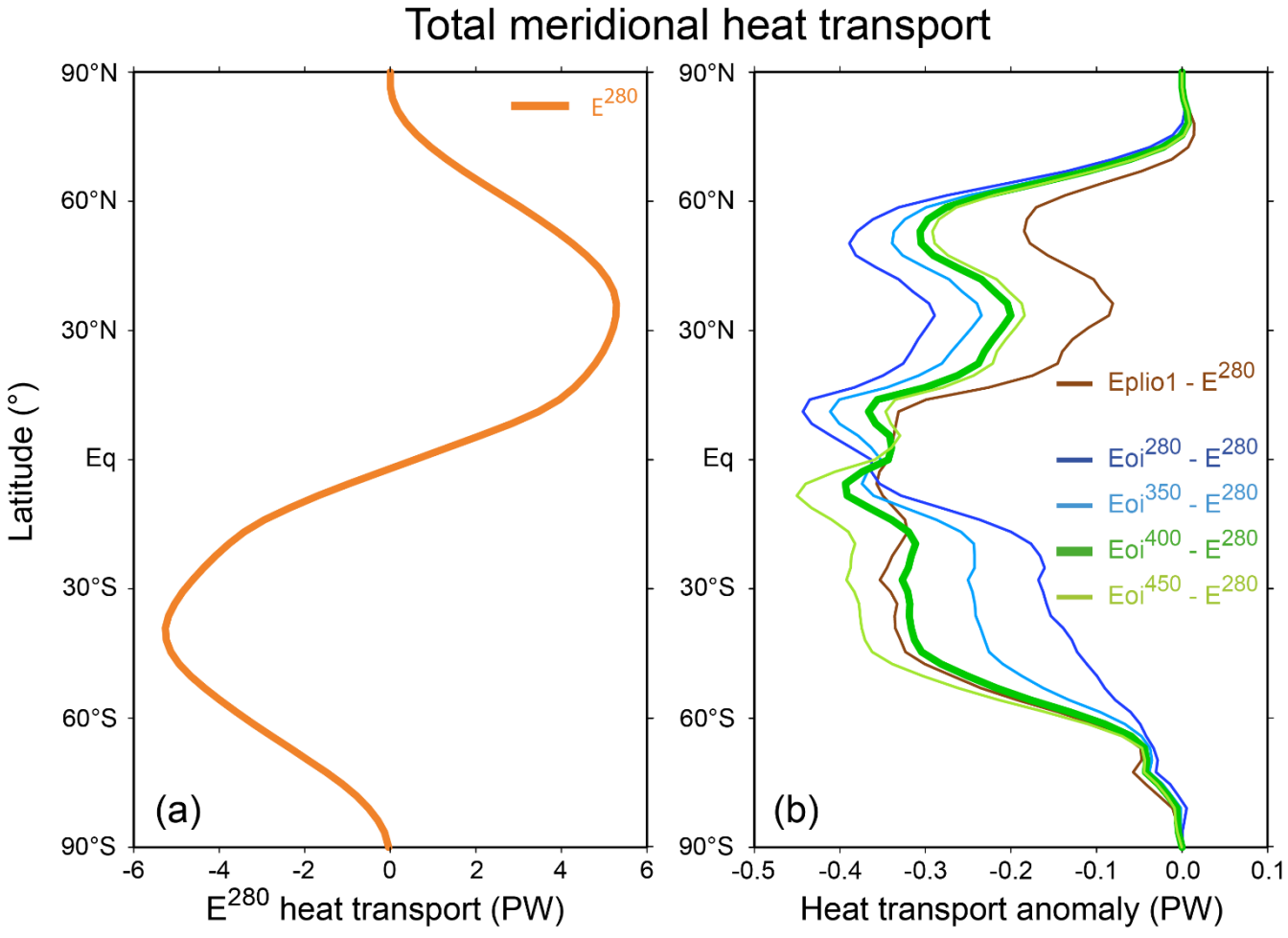

Figure 13: (a) The total meridional heat transport in E^{280}, as calculated from the top-of-atmosphere radiative transport, and (b) the anomaly between the Pliocene experiments and E^{280}. The core experiment, Eoi400, is shown in bold green.

615

https://doi.org/10.5194/cp-2020-17
Preprint. Discussion started: 19 February 2020
© Author(s) 2020. CC BY 4.0 License.

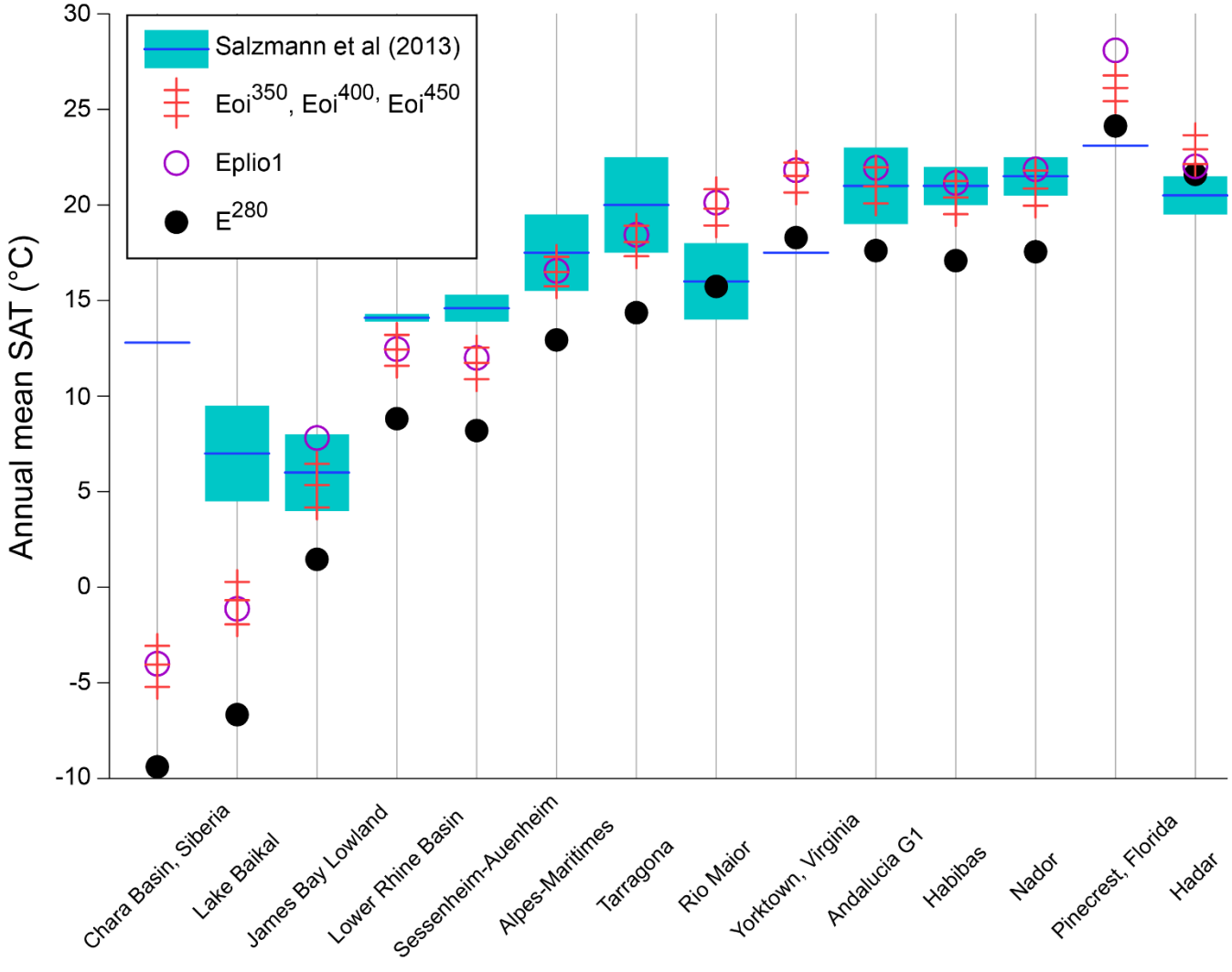

Figure 14: Comparison of annual mean surface air temperatures derived from proxy data (Salzmann et al., 2013) and those from model experiments. Proxy data are indicated by the dark blue line and the uncertainty range by light blue. The three red marks represent, from top to bottom, E^{450}, E^{400} and E^{350}.

620

https://doi.org/10.5194/cp-2020-17
Preprint. Discussion started: 19 February 2020
© Author(s) 2020. CC BY 4.0 License.

Climate of the Past Discussions
Open Access
EGU

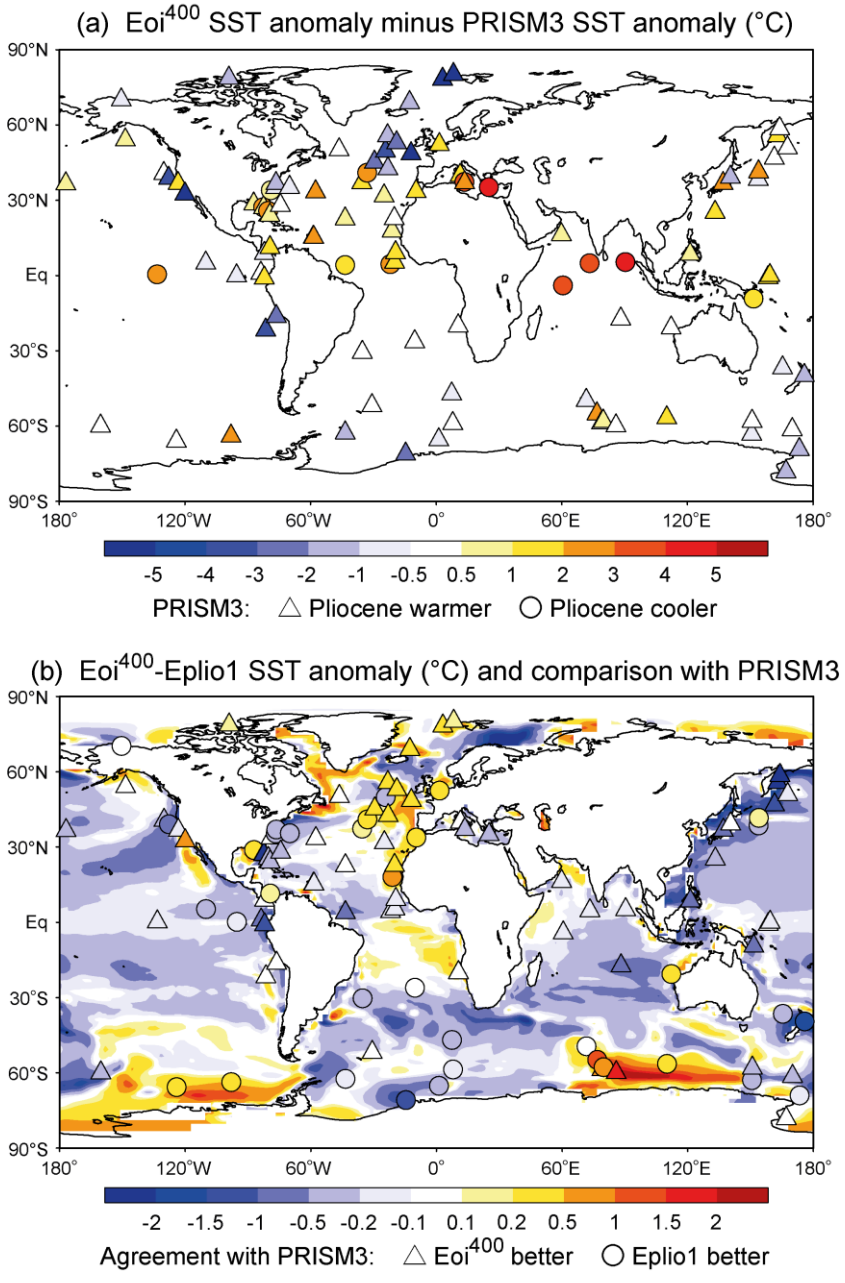

Figure 15: (a) Comparison of annual mean model SST anomalies and PRISM3 proxy data SST anomalies. Blue (red) indicates that model SST anomalies are smaller (greater) than those of proxy data. The shape of the symbols indicates whether proxy data suggests higher (triangle) SST in the Pliocene or lower (circle). (b) The difference between PlioMIP1 and PlioMIP2 SST. The shape of the symbols at PRISM3 locations indicates whether PlioMIP2 agrees better with proxy data (triangle) or whether PlioMIP1 agrees better (circle).

https://doi.org/10.5194/cp-2020-17
Preprint. Discussion started: 19 February 2020
© Author(s) 2020. CC BY 4.0 License.

Climate of the Past Discussions

Expt	Land-sea mask	Topography	Vegetation	Ice sheet	CO_2 (ppm)	Integration length (years)
E^{280}	Local modern	Local modern	Local Pre-Ind	Local Pre-Ind	280	2,220
E^{400}	Local modern	Local modern	Local Pre-Ind	Local Pre-Ind	400	3,000
E^{560}	Local modern	Local modern	Local Pre-Ind	Local Pre-Ind	560	3,920
Eplio1	PRISM3	Local modern + PRISM3 anom	PRISM3	PRISM3	405	4,000
Eoi^{280}	PRISM4	Local modern + PRISM4 anom	PRISM3	PRISM4	280	2,500
Eoi^{350}	PRISM4	Local modern + PRISM4 anom	PRISM3	PRISM4	350	3,000
Eoi^{400}	PRISM4	Local modern + PRISM4 anom	PRISM3	PRISM4	400	4,000
Eoi^{450}	PRISM4	Local modern + PRISM4 anom	PRISM3	PRISM4	450	3,000

Table 1: Boundary conditions, CO_2 levels and model integration length for each experiment in the present study.

CH_4	760ppb
N_2O	270ppb
O_3	Local modern
Solar constant	1365 W/m^2
Eccentricity	0.016724
Obliquity	23.446°
Perihelion	102.04°

Table 2: Settings common to all experiments in the present study. These refer to the last 1000 years, before which the following settings were used: 863.303ppb CH_4, 279.266ppb N_2O, 1366.12 W/m^2 solar constant.

https://doi.org/10.5194/cp-2020-17
Preprint. Discussion started: 19 February 2020
© Author(s) 2020. CC BY 4.0 License.

Climate of the Past Discussions

Expt	Global SAT (°C)	Global ΔSAT (°C)	North SAT (°C)	Tropical SAT (°C)	South SAT (°C)	TOA En Bal (W/m^2)	Global Precip (mm/dy)	Global SST (°C)	Global ocean T (°C)	AMOC Index (Sv)
E^{280}	12.8	0.0	-11.4	23.0	-18.4	0.88	2.69	17.0	1.91	19.5
E^{400}	14.8	2.0	-8.1	24.7	-15.3	0.96	2.79	18.4	2.54	18.7
E^{560}	16.8	3.9	-4.2	26.5	-12.7	1.02	2.90	19.9	3.40	17.8
Eplio1	16.3	3.5	-3.0	25.7	-12.3	0.85	2.87	19.2	3.44	17.8
Eoi^{280}	13.9	1.1	-7.7	23.5	-15.0	0.80	2.74	17.5	2.12	20.2
Eoi^{350}	15.1	2.3	-5.7	24.6	-12.2	0.83	2.81	18.4	2.69	20.0
Eoi^{400}	15.9	3.1	-4.4	25.4	-12.0	0.84	2.86	19.0	3.09	20.0
Eoi^{450}	16.6	3.8	-3.2	26.0	-11.0	0.84	2.90	19.6	3.46	19.8

Table 3: Global mean and other values for each experiment, averaged over the last 100 years. 1) Experiment name, 2) Global surface air temperature, 3) Global surface air temperature anomaly with E280 as the reference, 4) Surface air temperature averaged over latitudes 60°N-90°N, 5) Surface air temperature averaged over latitudes 30°S-30°N, 6) Surface air temperature averaged over latitudes 90°S-60°S, 7) Energy balance at the top of the atmosphere, 8) Global precipitation, 9) Global sea surface temperature, 10) Global ocean temperature averaged across all depths, 11) AMOC index. The AMOC index is averaged over the last 500 years to remove large centennial variability, as seen in Figure 2.

Experiment	Global	90°N-60°N	30°N-30°S	60°S-90°S
Eplio1	1.05	-1.28	2.19	0.04
Eoi^{280}	-0.76	-3.03	0.23	-1.08
Eoi^{350}	0.14	-4.43	1.21	-0.35
Eoi^{400}	0.76	-1.92	1.88	0.20
Eoi^{450}	1.31	-1.40	2.43	0.74

Table 4: The difference between the annual mean SST anomaly (from E^{280}) of each experiment and the equivalent from the PRISM3 proxy data. Positive values signify that the increase in model SST is greater than the increase in proxy SST. Units are °C. The PRISM3 proxy data were used as SST boundary conditions for AGCM experiments in PlioMIP1.